Diffusion of Small Molecules in Amorphous Glassy Polymers

A thesis submitted in partial fulfilment of the requirements for the Degree of Bachelor of Science (Honours)

by

RICHARD HUMFRY HENCHMAN

DEPARTMENT OF THEORETICAL CHEMISTRY

UNIVERSITY OF SYDNEY

NOVEMBER, 1995

ACKNOWLEDGEMENTS

I must thank Professor Tony Haymet for allowing me to study in the Department of Theoretical Chemistry.

I am especially grateful and indebted to Bob Gilbert for being my supervisor for this project. Our productive and inspiring conversations were without doubt the foundation stone of the project.

Mike Greenfield and Doros Theodorou (University of California, Berkeley) also deserve special mention for very generously providing the simulation data on which this project is based and explaining to me their work.

The following people must also be thanked: Matthew, for his experimental results and many discussions about aspects of the project; Emma, for ensuring that I didn't spend all my time talking to Bob, and all the other P/T Honours students, Max, Karina, Sophie and Feryal for their comradeship in this challenging year; Rob L, for his constructive, polite and confidence-building comments; Josh, for his idea-churning conversations, his Gary Larson comics and getting off the computer when I needed to use it; Hans, for those loud conversations about niks; Jelica, for keeping me informed of what was happening in the labs each week; Rob B, for the soccer tips and the ankle reconstruction; Sudarko and the others, for letting me move into their office; the others in the Polymer Group for being good company and for the help that they provided; everyone else in the Physical/Theoretical Department for their support.

TABLE OF CONTENTS

quem neque fama deum nec fulmina nec minitanti
murmure compressit caelum, sed eo magis acrem
irritat animi virtutem, effringere ut arta
naturae primus portarum claustra cupiret.
ergo vivida vis animi pervicit, et extra
processit longe flammantia moenia mundi
atque omne immensum peragravit mente animoque,
unde refert nobis victor quid possit oriri,
quid nequeat, finita potestas denique cuique
quanam sit ratione atque alte terminus haerens.

[whom neither talk of the gods nor thunderbolts checked,
nor the sky with its vengeful roar,
but all the more spurred the fierceful spirit of his mind
to strive to first break through the close-set bolts of nature.
And so it was that the lively force of his mind prevailed,
and he passed on far beyond the fiery walls of the world,
and in mind and spirit traversed the boundless universe;
whence in victory he brings us tidings what can come to be
and what cannot,
and how each thing has its power limited
and its deep-set boundary stone.]

(Lucretius, *De Rerum Natura*, Book I, 68-77)

Chapter 1

Introduction

1.1 Aim and Motivation

Today's demand for materials with specific properties is rapidly overtaking the available technology, especially in the *understanding* of why many materials have the properties they do. The diffusivity of small molecules in polymers is one such property. The aim of this project is to model the diffusion process of small molecules in glassy polymers. This is to enable a greater understanding of such systems, especially concerning the details of the transport mechanism, what factors it depends on and why diffusion coefficients are the size they are. Such models also assist in the interpretation of experiments that measure diffusion rates.

Small diffusing molecules are termed *penetrants*. One of the assumptions assumed in this work is that over large enough length scales, penetrants follow random paths. It has been shown that there is no long-range correlation in structure for amorphous polymers (Kreituss and Frisch, 1981), validating the random walk assumption. This randomness is equivalent to assuming that penetrants follow Fickian diffusion, for which Eq. 1.1 holds. This allows diffusion to be quantified by a single number, the diffusion coefficient.

$$J = D\nabla c \tag{1.1}$$

J is the penetrant flux, D the diffusion coefficient and ∇c the penetrant concentration gradient. This is one of the ways in which D can be defined. The other definitions utilise stochastic theory (Chandrasekhar, 1943) (see Eqs. 4.10, 4.11, 5.1).

The model is aimed at glassy polymers, in which polymer chain motions are essentially frozen (Rigby and Roe, 1987,90; Roe, 1994; Takeuchi and Roe, 1991), for the following reasons. Firstly, they are much less understood than rubbery polymers, since diffusion, being much slower in these more rigid structures, is both harder to measure experimentally and simulate computationally. Secondly, many polymer products are glassy. It is of prime importance to know how diffusivity of small molecules relates to the chemical constitution and morphology of the polymer so that a

polymer that is desired to be permeable, impermeable or even selective to the passage of small molecules can be designed. This selectivity property is especially pertinent to glassy polymers, for which it has been found that the rate of diffusion is sensitively dependent on the size of the small molecule (e.g. Stannett *et al.*, 1968). Thirdly, many polymers in their manufacture become glassy at high conversion. For conversion to go to completion, remaining monomer must diffuse around to reactive chain ends to continue propagation. Residual unreacted monomer is a waste and possibly an environmental hazard. This rate of monomer diffusion is important because it is so slow in glassy polymers that is the rate determining step for propagation (e.g. Gilbert, 1995).

This work concentrates on modelling diffusion of *small* gas molecules, such as methane, at very *low* concentration. This allows the reasonable assumption that small molecules can be approximated by Lennard-Jones spheres. However, it may not hold for larger molecules such as typical polymer monomers, such as methyl methacrylate, whose asphericity and internal degrees of freedom may become significant. Also, sparsely spaced penetrants can be reasonably assumed not to perturb the polymer matrix significantly or interact with each other. Finally, most of the literature with which the model can be compared and constructed from concerns small gas molecules.

This project first describes the various approaches in the literature that have been used to assist understanding penetrant diffusion in polymers and which will be used in the development of a model for diffusion. These approaches are theoretical models, experiments and computer simulations.

1.2 Basic Mechanism for Modelling

The distribution and dynamics of unoccupied volume (volume unoccupied by polymer when treated as having hard-sphere van der Waals radii) is critical to penetrant diffusion. Thus penetrant diffusion is strongly influenced by polymer mobility, which itself is strongly dependent on temperature, density and penetrant concentration (or equivalently, polymer conversion). Lowering temperature, raising density or decreasing penetrant concentration lowers polymer mobility. In rubbery polymers, in which polymer mobility is reasonably high, penetrant diffusion is assisted by the unoccupied

volume redistributions (e.g. Pant and Boyd, 1993). However, at around about the glass transition and below, polymer motion becomes frozen in, fixing cavities of unoccupied volume in space except for a few minor fluctuations (Rigby and Roe, 1987, 1990; Roe, 1994; Takeuchi and Roe, 1991; Greenfield and Theodorou, 1993). In order for penetrants to diffuse now, they must jump from cavity to cavity, a jump likely to involve a significant activation energy barrier. Barrer (1937,39a,b) was the first to conjecture these jumps in dense polymers. Such jumps have been observed in molecular dynamics simulations (Takeuchi, 1990a). The change in behaviour of D with temperature measured experimentally (e.g. Fig. 3.2; Ehlich and Sillescu, 1990) at the glass transition also points towards a change in the diffusion mechanism in glassy polymers.

1.3 Previous Models, Experiments and Computer Simulations

There are three main types of models for these systems. The dual-mode sorption model (e.g. Stern and Frisch, 1981) assumes that penetrants can exist in either of two phases, each with different diffusive properties. The free volume models (e.g. Fujita, 1961; Vrentas and Duda, 1977a-c; Vrentas and Vrentas, 1993) assume that the probability of a diffusive jump is proportional to a critical amount of free volume accumulating adjacent to the penetrant for it to jump into. Finally there are the molecular models (Brandt, 1959; DiBenedetto, 1963; Pace and Datyner, 1977a-c). They calculate the energy for an assumed specific simplified polymer motion of an energy-activated jump of the penetrant. Pace and Datyner (1977a,c) also estimate an Arrhenius "frequency factor" and jump length to give a diffusion coefficient by assuming an Arrhenius rate coefficient of jumping and stochastically occurring jumps.

Experiments provide few details of the mechanism of diffusion. Their principal results are variation of diffusion coefficient with temperature (e.g. Ehlich and Sillescu, 1990), penetrant concentration (Frick *et al.*, 1990) or pressure and penetrant size (Koros *et al.*, 1988). There are few experimental results for diffusion of small molecules in glassy polymers due to the difficulty of measuring such small diffusion coefficients (10^{-10} - 10^{-16} cm^2 s^{-1}). We are looking to compare the model with diffusion coefficients

of tracer dyes used in forced Rayleigh scattering experiments currently being performed on methyl methacrylate at high to full conversion (Tonge, in progress).

The main source of information that will be used for the modelling in this project is computer simulation, since it is able to describe the diffusion process on an atomistic scale. This, of course, comes at a price of the size of the system that can be represented. There are two types of computer simulation useful for the diffusion process. Molecular dynamics (MD) simulations (Takeuchi, 1990a,b; Takeuchi and Okazaki, 1990,93; Takeuchi *et al*., 1990; Sok *et al*., 1992; Müller-Plathe, 1991,92; Müller-Plathe *et al*., 1992,93a,b; Boyd and Pant, 1991-93; Trohalaki *et al*., 1989; Tamai *et al.*, 1994, Sonnenburg *et al.*, 1990) track the behaviour of a system through time. While they can provide quantitatively useful diffusion coefficients for penetrant diffusion in rubbery polymers, their short simulation timescales of 1-10 ns mean that they can only provide qualitative information in glassy polymers, since penetrant diffusion is too slow in these systems for its motion to be properly sampled. The second simulation method uses transition-state theory (TST) to calculate the rate coefficients of jumps (Gusev and Suter, 1993; Gusev *et al.*, 1993,94; Greenfield and Theodorou, 1993-95a,b). Stochastic simulations (e.g. June *et al.*, 1991) with timescales of up to 1 μs can use these rate coefficients to produce a macroscopic D (Gusev *et al.*, 1993).

1.4 A Model to Predict Diffusion Coefficients

For much of its analysis, the model to be proposed focuses on the work of Greenfield and Theodorou (1993-95a,b) for inspiration and insight. They use multidimensional TST incorporating polymer as well as penetrant degrees of freedom to calculate rate coefficients of jumps of a methane penetrant in glassy atactic polypropylene (PP) at 233 K. Final results from their work are yet to be published. It needs to be stressed that while their simulations are used as a guide, the model, when created, is intended to predict D's on its own. Despite the fact that the proposed model is designed for their system in particular, it is hoped that qualitative if not quantitative aspects of the model deduced in PP can be applied to other polymer-penetrant systems.

While Greenfield and Theodorou's work shows there to be a large distribution of possible jumps in the polymer, it assumed that an "average", "rate-determining"

jump can be found. Models are provided to quantify three parameters of this jump. These are l, the jump length, E_0, the critical energy required for the jump, and Q^+/Q, the ratio of transition state partition function to penetrant partition function. The TST formula (Eq. 4.12) is then used to obtain a rate coefficient, k. Stochastic theory (Eq. 5.1) then produces a diffusion coefficient, D. Possible modifications and improvements to the model are also discussed.

Chapter 2

Existing Models for Diffusion

2.1 Free Volume Model

One of the first models for diffusion of molecules in any condensed-phase system was to assume that the ability of molecules to diffuse depended on the amount of empty space in the system. The first functional form for such a relationship was observed experimentally by Doolittle (1951) in simple hydrocarbon liquids, which says that their fluidity, ϕ (inverse viscosity), proportional to the diffusion coefficient for Stokes-Einstein systems, is given by

$$\phi = A\exp\left[-bv_0 / v_f\right] \tag{2.1}$$

where A and b are constants, v_0 is the van der Waals volume of the penetrant, and v_f is the average free volume per molecule, given by the equation

$$v_f = v_m - v_0 \tag{2.2}$$

where v_m is the average volume per molecule in the liquid. Cohen and Turnbull (1959) were able to derive such an expression for D,

$$D = ga^* u\exp\left[-\gamma v^* / v_f\right] \tag{2.3}$$

where g is a geometric factor, a^* is approximately the penetrant diameter, γ corrects for free volume overlap, u is the molecule's gas kinetic velocity, and v^* is the critical free volume needed to form next to a penetrant into which it can permanently jump. This equation says that D is proportional to the chance of such a critical free volume forming. Fitting D to v_f by Eq. 2.3 is the simplest free volume treatment. It is assumed that the hole free volume can be redistributed with no energy barrier, so that each configuration of free volume is equally likely.

Fujita (1961) was the first to apply free volume theory to penetrant diffusion in concentrated polymers with suitable modifications. Vrentas and Duda (1977a-c; Vrentas and Vrentas, 1993) have since significantly developed its application to penetrants in polymers. Letting the number 1 refer to penetrant and 2 to polymer, their theory predicts that the self-diffusion coefficient of the penetrant is given by

$$D_1 = D_{01}\exp\left(\frac{-E}{RT}\right)\exp\left[\frac{-\gamma\left(\omega_1\hat{V}_1^* + \omega_2\xi\hat{V}_2^*\right)}{\hat{V}_{FH}}\right] \tag{2.4}$$

where E is the attractive energy holding the penetrant to its neighbours, D_{01} is a pre-exponential factor, γ is an overlap factor, ω_i is the mass fraction of component i, $\hat{V}_i^*$ is the specific critical hole free volume for component i, ξ is the ratio of the critical molar

volume of the solvent jumping unit to the critical molar volume of the polymer jumping unit, and $\hat{V}^*_{FH}$ is the average hole free volume per gram of mixture, defined by

$$\hat{V}^*_{FH} = \omega_1(K_{21} + T - T_{g1})K_{11} + \omega_2(K_{22} + T - T_{g2})K_{12} \qquad (2.5)$$

where K_{1i} and K_{2i} are free-volume parameters for component i and T_{gi} is the glass transition temperature of component i. The authors claim that the many parameters can all be evaluated in special circumstances, making the theory predictive (Vrentas *et al.*, 1989). However, in general there is difficulty in evaluating all parameters, particularly E, D_0 and ξ. Nevertheless, it is still a useful equation to fit to and correlate experimental data.

Free volume theories have been found to describe D's above the glass transition, but have been found to break down in the glassy region (e.g. Frick *et al.*, 1990) not predicting the levelling off at temperatures below T_g. Vrentas *et al.* (1988) claim that an extra term in the expression for $\hat{V}^*_{FH}$ fixes this. However, we believe that below the glass transition, the frozen polymer chains restrict the redistribution of free volume. For penetrants to diffuse in glassy systems, they must jump from one region of free volume to another over an energy barrier. The next two models attempt to take these aspects into consideration.

2.2 Dual-Sorption Model

Designed specifically for glassy polymers, the dual-mode sorption is not so much a predictive model but rather an explanation of why D's are concentration dependent. The model assumes that the penetrant gas dissolved in the polymer can be divided into two phases (e.g. Stern and Frisch, 1981). One phase consists of penetrant dissolved in the normal way, with the concentration, C_D, related to pressure, p, by Henry's law, which in the dilute limit is

$$C_D = k_D p \qquad (2.6)$$

where k_D is Henry's constant. Such a treatment is considered sufficient for rubbery polymers. The second phase consists of penetrants trapped in a fixed number of cavities in the polymer, characteristic of glassy polymers. The concentration for such penetrants, C_H, is given by a Langmuir isotherm

$$C_H = \frac{C'_H bp}{1 + bp} \tag{2.7}$$

where C'_H is a "hole saturation" constant and b is a "hole affinity constant". Rapid exchange is postulated to occur between the two populations. The total concentration is given by the sum of these. Each phase is also assumed to have a D associated with it, D_D and D_H respectively.

2.3 Activation-Energy Models

These models calculate the activation energy, E, and pre-exponential factor, D_0, for an assumed molecular process, giving D by an Arrhenius expression

$$D = D_0 \exp(-E / RT) \tag{2.8}$$

The first such model was by Brandt (1959). It attempts to calculate the energy for two polymer chains, assumed to be parallel, to be forced apart, as seen in Figure 2.1, so as to allow a penetrant to squeeze between in a direction perpendicular to the page.

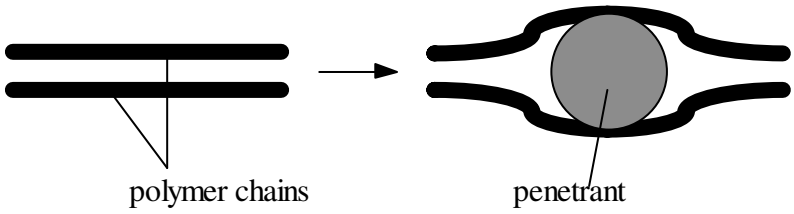

Figure 2.1: Sketch illustrating the assumed activated mechanism of Brandt, in which two polymer chains move apart to allow a penetrant to fit between them.

E is assumed to have three components. These are an intermolecular repulsive term between expanding chains and their neighbours, intramolecular terms due to bending and rotating the chains as they twist, and a thermal term. The intermolecular component is taken as the change in volume multiplied by the internal pressure of the polymer. The intramolecular component is taken as rotations of a hindered rotor. Brandt assumes that there are two degrees of freedom for each chain segment and minimises the total energy with respect to the total number of segments. Barrer's theory (1957) is used to calculate

D_0. Apparent activation energies for various parameter choices are compared with experiment for system of ethane in polyethylene. The model's energies are 25-70 % lower than the experimental value of 56 kJ mol^{-1}. While all parameters are evaluated, it is done in a rather approximate way. penetrant

The second molecular model was by DiBenedetto (1963). He assumed that penetrants moved parallel to and down the centre of a bundle of four, effectively crystalline, polymer chains as shown in Figure 2.2. In the normal state, polymer chains wrap around the penetrant. The chains must expand away from the penetrant so that the penetrant can slide down the tube parallel to the chains. The energy to do this is taken as the weakening of van der Waals bonds between each polymer chain. The activation energies obtained were in reasonable agreement with experimental data. However, the model requires experimental input to determine how far each motion is.

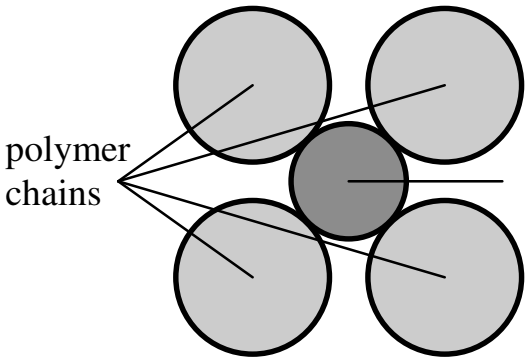

Figure 2.2: Sketch illustrating position of penetrant in relation to polymer chains. The penetrant moves perpendicular to the page parallel to the polymer chains.

Pace and Datyner (1977a-c) took their molecular mechanism of diffusion to be a combination of the Brandt and DiBenedetto mechanisms. The penetrant is assumed to be able to move down the tube parallel to chains, similar to the DiBenedetto model, but without any energy barrier. However, at the end of these tubes are entanglements. The Brandt model of jumping between chains must now occur for the penetrant to exit the tube, a jump requiring energy. The components of this energy are taken as working against the attractive energy between polymer chains, and twisting the polymer chains, which makes them bend away. The rate coefficient of jumping is obtained from a modification of Barrer's theory (Barrer, 1943). The length of a jump is taken as the length of a tube. A rough estimate for this is obtained from the concentration of

entanglements in the polymer (Pace and Datyner, 1977c), giving jump lengths over the large range of 1 - 400 nm. Assuming jumps occur stochastically, a diffusion coefficient is obtained from stochastic theory (Chandrasekhar, 1943) using Eq. 5.1.

Comparisons are made between the apparent activation energy predicted by the model and experimental activation energies for a wide range of polymers as a function of penetrant diameter. While the agreement is quite good for non-vinylic polymers (Pace and Datyner, 1977b) the theoretical values are too large for vinylic polymers (Pace and Datyner, 1977c), as can be seen in Figure 2.3.

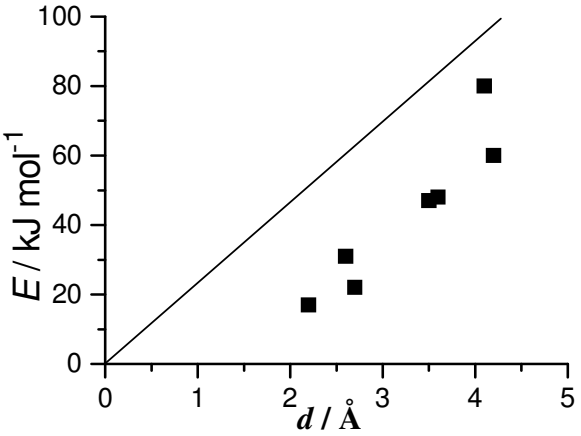

Figure 2.3: Comparison with experiment (dots; Meares, 1954,1957) of the theoretical apparent activation energies, E_{app}, (solid line) versus penetrant diameter, d, for glassy polyvinyl acetate (Pace and Datyner, 1977c). Shifting the curve right by 1.5 nm would produce agreement between the two.

A possible source of this deviation, as is discussed in this work's modelling of diffusion in Chapter 5, is that there are already percolating pathways through polymers. So penetrants smaller than a certain size can travel through the polymer encountering negligible energy barriers. Pace and Datyner assume that there is no unoccupied volume between polymer chains before they separate. If there was an initial separation of a given distance, this would allow the curve in Figure 2.3 to be shifted to the right by that distance, since the chains now do not have to separate as much for a given penetrant.

To summarise the molecular models, at best, they give reasonable values for activation energies of diffusion, but their theory for predictive theory for D's is incomplete. The models themselves are rather large simplifications of reality, they assume semi-crystalline polymers, and the evaluation of the model parameters is in

some cases rather approximate. Furthermore, they have no real evidence, especially on a molecular level, of their postulated diffusion mechanisms. What is needed are molecular level details of the diffusion mechanism. These can now be provided by computer simulations, discussed in Chapter 4.

Chapter 3

Experimental Measurements of Diffusion Coefficients

3.1 Usefulness of Experiments

Experiments are currently unable to directly give detailed molecular-level information of the mechanism of penetrant diffusion in polymers. NMR studies of polymer chain dynamics (e.g. Schaefer *et al.*, 1990), neutron scattering probing of polymer structure (e.g. Furuya *et al.*, 1994), and o-positronium annihilation data on unoccupied volume (Lind *et al.*, 1986) can provide related information, but in general experiments are not a good starting point for elucidating a mechanism to model. However, experiments can measure penetrant D at different temperatures, penetrant concentrations and in polymer matrices. Therefore, models need to be able to predict or at least correlate D with these parameters so that they can be compared with experiment. Since the model in this work is aimed towards infinitely dilute penetrants in glassy systems, only D's themselves and their behaviour over glassy temperature ranges can be compared with experiment. The problem here is that D's in this region are extremely small, varying from 10^{-6} down to at least 10^{-16} cm^2 s^{-1}, their slowness making them hard to measure. Thus experimental data for these systems is scarce and can be unreliable.

3.2 Experiments for Measuring *D*

There are three main approaches to measuring D. The first of these are pulsed-field gradient NMR methods (PFG NMR) (e.g. Pickup and Blum, 1989; Piton *et al.*,

1993). They require penetrants to have nuclei with non-zero spin, such as H or C. They can measure D's only down to about 10^{-11} cm^2 s^{-1}, limited by the NMR timescale, and so cannot probe glassy regions of most polymers. The basic principle of PFG NMR is that application of a pulsed linear magnetic field gradient to a system of nuclear spins will make them precess at different frequencies depending on the strength of the field. Then another pulse sequence and another pulsed field gradient are applied, so as to rephase the spin of the nuclei. However, if the nuclei have moved, they will not be completely refocused, reducing the intensity of the outputted NMR signal. By varying the time for which the field gradient is applied, δ, D is extracted from the equation

$$I(\delta)/I(\delta=0)=\exp\left(-Df(\delta)\right) \tag{3.1}$$

where I is the NMR signal intensity and $f(\delta)$ includes constants determined by the experimental system. Figure 3.1 shows the results for such an experiment as a function of temperature and polymer conversion. It can be seen that Arrhenius behaviour is obtained for these systems. However, this behaviour, being measured in rubbery systems, is not helpful in modelling glassy systems.

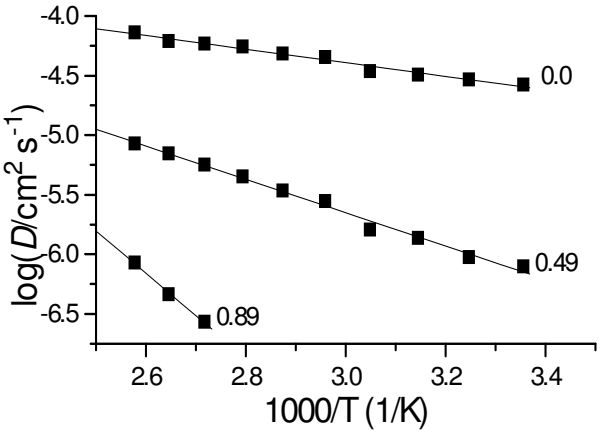

Figure 3.1: D of toluene in polystyrene plotted as a function of polymer conversion, (0.0, 0.49, 0.89), and temperature. These points were measured by PFG NMR (Pickup and Blum, 1989).

The second method is gas permeation, in which a gas pressure, p, is applied to one side of a polymer membrane of width l, setting up a steady state flux through the polymer. Since the flux is given by $J = P\nabla p$, the permeability, P, is given by

$$P=\frac{Jl}{p}. \tag{3.2}$$

D is obtained from lag time experiments, in which the steady-state flux is extrapolated back to zero, the time at which this occurs being the lag time, θ. The formula used (e.g. Gusev *et al.*, 1994) is

$$D = \frac{l^2}{6\theta}. \tag{3.3}$$

However, this approach might not be reliable for glassy polymers (Paul and Koros, 1976). This method requires that penetrants have a certain degree of solubility in the polymers. It is capable of measuring D down to about 10^{-11} cm^2 s^{-1}, although with diminishing accuracy. The slower D is, the longer times required for penetrants to diffuse a given distance, making this technique prohibitively slow. Experimental D's for different penetrants are shown in Figure 5.12 (Koros *et al.*, 1988).

The third technique, forced Rayleigh scattering (FRS) (e.g. Huang *et al.*, 1987, Zhang *et al.*, 1986) is able to measure much smaller D's, down to 10^{-16} cm^2 s^{-1}, since it measure D's over much smaller length scales. It involves the measurement of D's for tracer dye molecules in the polymer, rather than for the penetrant of interest. Two coherent laser beams intersecting at the sample of dye-containing polymer produce a sinusoidal interference pattern. Since laser light converts the tracer dye to a photoproduct with different spectral properties, a sinusoidal pattern of photoproduct and dye concentration is formed in the polymer. This system now has the properties of an optical grating. A third laser passed through the sample is diffracted by it. As the concentration gradient of dye and photoproduct evens out due to diffusion, the intensity of the diffraction pattern decreases. The intensity, $I(t)$, as a function of time is fitted by the equation

$$I(t) = \left[A\exp(-t/\tau_1) + B\exp(-t/\tau_2)\right]^2 + C \tag{3.4}$$

where A, B and C are constants. From this, the relaxation times of dye and photoproduct, τ_1 and τ_2, are obtained. Their D's are obtained from the equation

$$D_i = \frac{\lambda^2}{16\pi^2\tau_i \sin^2(\theta/2)} \tag{3.5}$$

where λ is the laser wavelength and θ is the angle between laser beams. Free volume theory is then used to obtain the D of the actual penetrant of interest by the equation (e.g. Frick *et al.*, 1990)

$$\log(D_{dye}) = \frac{V_{dye} M_{dye}}{V_{pen} M_{pen}} \log(D_{pen}) + b \tag{3.6}$$

where V are molecular volumes, M are molecular weights and b a constant. Such a relationship can be established by measuring D's of both species by another technique such as PFG NMR, but applying it through the glass transition may be inaccurate.

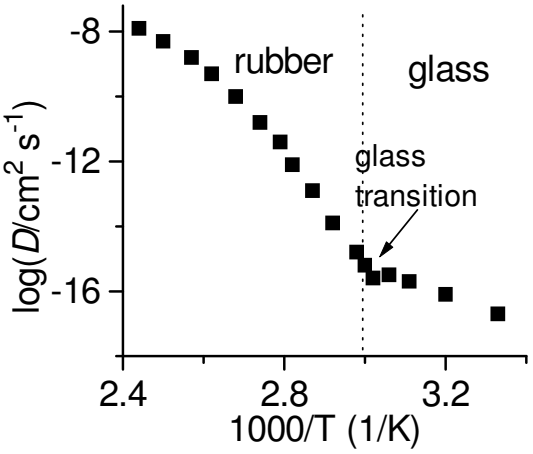

Figure 3.2: Diffusion coefficient of the tracer dye TTI (tetrahydrothiophene-indigo) measured by FRS as a function of temperature (Ehlich and Sillescu, 1990) across the glass transition, at which a change in its behaviour is seen. The polymer matrix is polystyrene with 10 % tricresyl phosphate.

Shown in Figure 3.2 is a measurement of D by FRS as a function of temperature (Ehlich and Sillescu, 1990). D drops rapidly with decreasing temperature as polymer motions become more restricted and the amount of free volume decreases. The rubbery part of the plot can be fitted using an equation based on free-volume theory, the Williams-Landel-Ferry (WLF) equation (Williams *et al.*, 1955),

$$\log\left[\frac{D(T)}{D(T_g)}\right] = \frac{C_1(T - T_g)}{C_2 + T - T_g} \tag{3.7}$$

where T_g is the glass transition temperature of the polymer and C_1 and C_2 are constants. As mentioned in chapter 2, deviation from this curve in the glass is thought to be due to the break-down of free volume theory. The behaviour in the glassy region looks to be Arrhenius.

Measurements of D versus polymer conversion, or equivalently, penetrant concentration, can be reasonably fitted by the Vrentas free-volume model (Vrentas and

Duda, 1977a-c, Vrentas and Vrentas, 1993). Data from such a measurement is shown in Figure 3.3 (Frick *et al*., 1990).

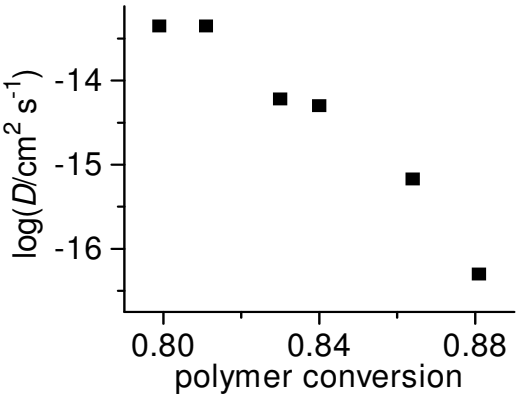

Figure 3.3: Plot of *D* of the tracer dye aberchrome 580 versus polymer weight fraction measured by FRS for polystyrene, the rest being toluene (Frick *et al.*, 1990). Each point is measured at the glass transition temperature for each system. It can be fitted by Vrentas *et al.*'s free volume model.

Tonge (in progress) is currently measuring *D* of the tracer camphorquinone by FRS in poly(methyl methacrylate) at glassy conversions (Figure 3.4). While work measuring *D* over a wider polymer conversion range is yet to be completed, there are indications that the penetrant's *D* has levelled off.

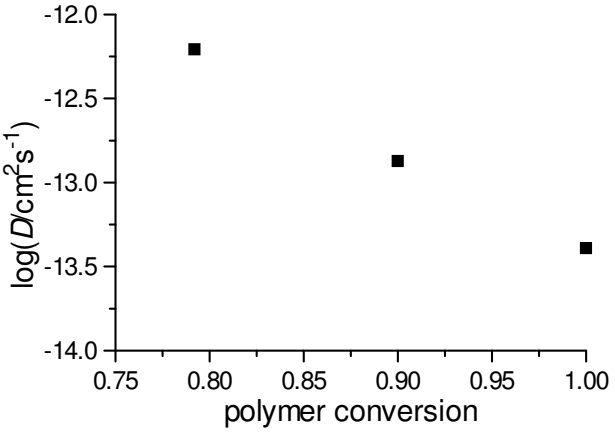

Figure 3.4: Scaled *D* for methyl methacrylate in poly(methyl methacrylate) versus polymer conversion at 298 K (Tonge, 1995). The tracer dye used was camphorquinone.

It can be seen that experiments provide trends of *D* with temperature, polymer conversion and penetrant. However, they fail to give insight into the actual mechanism of diffusion. Computer simulations, on the other hand, are able to do this.

Chapter 4

Computer Simulations of Small Molecule Diffusion

4.1 Usefulness of Computer Simulations

Computer simulations of diffusion of small molecules in glassy polymers can show exactly what is occurring on a molecular scale. The system can be carefully controlled, with a wide range of systems capable of being simulated.

However, how closely the simulation replicates reality depends on the level of theory used. Simulations of penetrants in polymers have either treated the system as hard spheres connected by fixed bonds (Sonnenburg *et al.*, 1990) or used an empirical force field (authors mentioned below). Most simulations have used the latter. Hardware limitations restrict computers to simulating very small molecular level systems if a reasonable level of reality and manipulation is allowed. Periodic boundary conditions (PBC) are enforced to eliminate surfaces. In the trade-off between the size of the system and how much it can be manipulated, most current polymer simulations strike a balance of using an empirical force field with a simulation box of side 20 - 50 Å. What is done with the systems is discussed in the following section.

There are two principal applications of computer simulations to diffusion in polymers, molecular dynamics (MD) (Takeuchi, 1990a,b; Takeuchi and Okazaki, 1990,93; Takeuchi *et al*., 1990; Sok *et al*., 1992; Müller-Plathe, 1991,92; Müller-Plathe *et al*., 1992,93a,b; Boyd and Pant, 1991-93; Trohalaki *et al*., 1989; Tamai *et al.*, 1994), in which the system is evolved in time, and transition state theory (TST) (Gusev and Suter, 1993; Gusev *et al.*, 1993,94; Greenfield and Theodorou, 1993-95a-d), which can calculate rates of certain processes, in particular, the jump. Polymers examined include polyethylene (PE), atactic polypropylene (PP), poly(dimethylsiloxane) (PDMS), polyisobutylene (PIB), and bisphenol-A-polycarbonate (PC). Penetrants examined include He, H_2, Ar, O_2, N_2, CH_4, H_2O, CO_2 and CH_2CH_2OH. The components of the empirical potential used are bond stretches (some authors used the *SHAKE* algorithm

(Ryckaert *et al.*, 1977) to constrain bonds (Sok *et al.*, 1992; Müller-Plathe *et al.*, 1993a,b)), given by

$$V(r) = \tfrac{1}{2} k_r (r - r_0)^2 \tag{4.1}$$

where r_0 is the equilibrium bond length and k_r the force constant, bond angle stretches,

$$V(\theta) = \tfrac{1}{2} k_\theta (\theta - \theta_0)^2 \tag{4.2}$$

where θ_0 is the equilibrium bond angle and k_ϕ the force constant, torsional potentials,

$$V(\phi) = k_\phi \left[1 + \cos(n\phi - \delta)\right] \tag{4.3}$$

where δ is a phase shift, n a multiplicity factor and k_ϕ is the force constant, non-bonded Lennard-Jones interactions, truncated at large distances,

$$V_{ab}(r) = 4\varepsilon\left[\left(\sigma_{ab} / r\right)^{12} - \left(\sigma_{ab} / r\right)^{6}\right] \tag{4.4}$$

where the Lorentz-Berthelot mixing rules are used for to give the appropriate Lennard-Jones diameter, σ, and energy parameter, ε, for interactions between different atoms

$$\sigma_{ab} = \tfrac{1}{2}(\sigma_a + \sigma_b) \tag{4.5}$$

$$\varepsilon_{ab} = (\varepsilon_a \varepsilon_b)^{1/2} \tag{4.6}$$

and, in the case of PDMS, a Coulombic electrostatic potential,

$$V(r) = \frac{q_i q_j}{4\pi\varepsilon_0 r}. \tag{4.7}$$

Densities, except when they are intentionally varied, are chosen to be the experimental value of the bulk polymer. Temperatures at which the simulations are done range from 90 to 420 K, with most done at 298 K. Most of the simulations were done at temperatures at which polymers were rubbery. The number of penetrants present in the system, varies from one up to about twenty. Techniques to generate polymer structures are listed in Appendix A.

A common approximation made is the united atom approximation, in which clusters of atoms are replaced by a single atom in order to reduce the total number of atoms to simplify computations. This is principally done for carbons and the hydrogens attached to them. It is reasonable for methyl (CH_3) groups, due to symmetry and its relative ease to rotate. However the approximation is not as good for CH_2 and CH groups due to their lower symmetry.

4.2 Molecular Dynamics

Molecular dynamics simulations simulate the behaviour of a system over time. Given a potential function, this is done by solving Newton's equations, typically using the velocity Verlet algorithm (Verlet, 1967), which gives subsequent positions and velocities by these formulae

$$r(t+\Delta t) = 2r(t) - r(t-\Delta t) + \Delta t^2 F(t) \tag{4.8}$$

$$v(t) = \left[r(t+\Delta t) - r(t-\Delta t) \right] / (2\Delta t) . \tag{4.9}$$

Given the size of the box and the degree of realism of the polymer, current simulation times are of order 1-10 ns using timesteps of order 1 fs.

Diffusion coefficients of penetrants can be calculated either by the mean-squared displacements formula

$$D = \lim_{t\to\infty} \frac{< \left(r(t) - r(0) \right)^2 >}{6t} \tag{4.10}$$

or from the velocity autocorrelation function

$$D = \tfrac{1}{3} \int_0^\infty < v(t)v(0) > dt . \tag{4.11}$$

A number of interesting aspects of penetrant diffusion in polymers were observed in MD simulations. The first of these is the mechanism of diffusion. Takeuchi (1990a) saw that oxygen molecules, rattling around for long periods in cavities, would eventually jump to neighbouring cavities when polymer motions opened up a connecting neck between them. These jumps were found to be particularly well defined for glassy polymers and for larger penetrants. The size and frequency of these jumps seem to be significantly affected by the size of the penetrant and the nature of the polymer. The smaller the penetrant (for example, He) and the more rubbery the polymer (for example, PDMS), the more frequently jumps occur. A lot more noise set into their trajectories as well, making the jumps less well defined. As would be expected, *D*'s for smaller penetrants are also larger. However, at the other extreme, jumps of penetrants in glassy systems are quite well-defined. Jump lengths found vary from 2 - 20 Å. The

energetics of the jump have also been examined. Takeuchi examined one jump and found that once the connecting neck had opened up, a process requiring energy, the oxygen penetrant was able to slip through the formed neck without much of an energy barrier. However, an MD simulation by Müller-Plathe *et al*. (1993a) showed that the translational kinetic energies of the penetrants were above average for penetrants around the time of jumps, suggesting that penetrants still require some energy to perform successful jumps.

All MD simulations appear to have been able to produce Fickian diffusion (doubt can be cast on some early ones), except in glassy systems for which long enough times cannot be simulated to obtain the required random walks (Takeuchi, 1990a). Three time domains (e.g. Pant and Boyd, 1993) are found in mean squared penetrant displacement versus time plots, as shown in Figure 4.1.

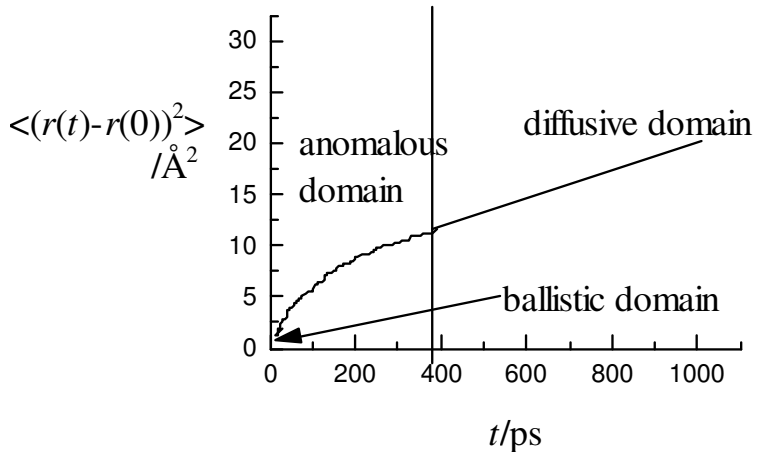

Figure 4.1: Typical plot of $<(r(t)-r(0))^2>$ versus time for diffusing penetrants, showing the three time domains. The ballistic domain shows up as a quick rise in displacement at very short times.

At very short times of the order 1 ps, penetrants execute ballistic motion as they rattle in cavities ($<(r(t)-r(0))^2>$ proportional to t^2). Anomalous diffusion, in which penetrants are still following correlated paths, then occurs up to times from as little as 10 ps up to at least 1 ns, depending on how fast the penetrant diffuses. The curve starts off steeply, since fast jumps present an easy way for a penetrant to move some distance, and then gradually levels off to a straight line, as slower jumps now can only help the penetrant move further. This time domain may extend even further for some systems, but this currently cannot be shown given the restricted simulation times. After this domain is the Fickian domain, in which $<(r(t)-r(0))^2>$ is proportional to t, with the proportionality

constant giving *D*. Some doubt needs to be placed on the earlier calculations of diffusion coefficients as to whether they simulated long enough times to reach the Fickian domain. The fact that the *D*'s measured by them were at least an order of magnitude too large, as would happen if the system were still the anomalous domain, and that later longer time simulations (Tamai *et al.*, 1994) found that diffusion was still anomalous at the end of these shorter time simulations, supports this.

MD's have been used to look at how *D* varies with temperature. Takeuchi and Okazaki (1990) found for O_2 in rubbery PE that the relationship appeared to be Arrhenius (Eq. 2.8) over a small range of temperature. Trohalaki *et al.* (1989) obtained a similar result for CO_2 in an n-alkane system. However, when interpreting data for the variation of *D* over a range of temperatures, it is important to note that the structure of the polymer also changes, gradually altering the mechanism of diffusion. Takeuchi and Okazaki build this idea in by assuming that ln*D* is proportional to the free volume fraction, v_f, the fraction of total volume unoccupied by polymer chains, where atoms are treated as hard spheres with the Lennard-Jones diameter. v_f also varies with temperature. This has the effect of making E_a consist of two components, one the activation energy of some diffusion process and the other a "thermal expansion term". Pant and Boyd (1993) also looked at *D* varying with *T* over a wider temperature range (still rubbery) for methane in PE and PIB. For PE, they found not Arrhenius behaviour but WLF behaviour (Eq. 3.7). Such a result is consistent with free volume theory. The fact that their results are similar to experimental data suggests that their findings are more likely to be correct. The result for PIB was not conclusive.

The influence of the amount and distribution of free volume has been investigated. Takeuchi and Okazaki (1993), by varying the density, verified the simple free volume theory equation for O_2 in PE (Eq. 2.3) They were also able to obtain the same relationship in the rather abstract case of varying v_f by artificially changing the bond angle of PE.

Polymer mobility was also examined. Takeuchi and Okakazi (1990) removed the barrier to torsional rotation, making the relaxation time of polymer torsion, τ_e, decrease by a factor of 30. However, the oxygen penetrant was found to diffuse only

twice as fast in such a system. A system of an infinite chain polymer was compared with a system of short chains. The presence of chain ends should increase polymer mobility. In the infinite chain system, τ_e was found to be half that in the short chain system, and *D* of oxygen was only slightly smaller.

The reason why many of the above features were investigated is that the early MD simulations predicted penetrant diffusion coefficients one or two order of magnitudes too large. As summarised by Müller-Plathe (1992), possible reasons could include using the united atom approximation, as large spheres will not pack as well as many small spheres, thus leaving more empty space. Finite chains used in simulations, being much shorter than real polymers, are more mobile. Polymer structures might not be properly equilibrated, with the resulting density being too low. The simulation of purely amorphous polymers might not correspond to real polymers that are assumed also to be amorphous. Crystallinity in real polymers lowers experimental *D*'s. Finally, simulation times might not be long enough to reach the Fickian time domain. Recent MD simulations have produced answers in reasonable accord with experiment. They have used better equilibration techniques, longer simulation times and either explicitly included all atoms (Müller-Plathe *et al.*, 1993a; Tamai *et al.*, 1994) or used the anisotropic united atom technique of Pant and Boyd (1992,93).

4.3 Transition State Theory

There is a large waste of computational time in MD simulations of diffusion, especially in glassy polymers, since penetrants are most of the time rattling around in cavities. In only a fraction of the total time do the important jump events actually occur. It would be particularly desirable to leave out the rattling time and just focus on the jumps. Transition state theory provides an approximate way of doing this. It enables calculating the rate coefficient, *k*, of each possible jump from cavity to cavity in a polymer microstructure.

If one looks at the region of the system's potential energy surface containing two minima, one in the reactant cavity and one in the product cavity, there will be a path of minimum energy connecting each minimum, termed the reaction path. This path

can be parametrised by a coordinate, termed the reaction path. Figure 4.2 shows the reaction path of the potential energy surface projected onto the reaction coordinate.

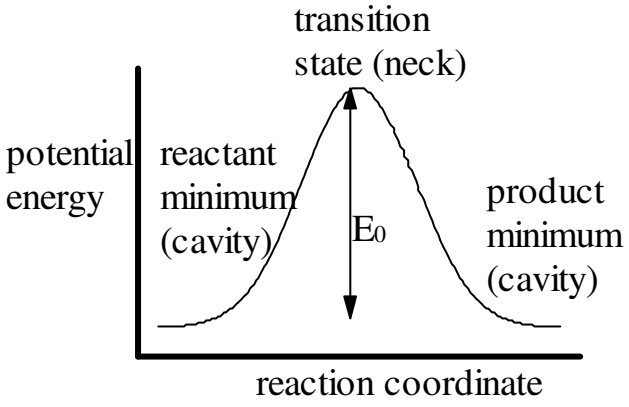

Figure 4.2: Potential energy along the reaction coordinate, the minimum energy path between reactant and product minima. The transition state is taken as the maximum on this path.

TST (e.g. Gilbert and Smith, 1990) assumes that a critical surface orthogonal to the reaction coordinate can be found such that every trajectory starting in the reactant minimum and passing through this surface does not recross the surface and goes on into the product minimum. A good approximation for the transition state is to have it at the maximum of the reaction path. The minimum of this transition state is a saddle point, since it is a maximum along the reaction coordinate, but a minimum with respect to all other coordinates. Symmetry in the system can make such saddle points second order and higher, that is, maxima with respect to two or more coordinates. However, there is unlikely to be any symmetry in amorphous polymer systems.

Another key assumption of TST is that of ergodicity. This states that a system with any initial energy distribution will be randomised amongst the degrees of freedom to that of a microcanonical equilibrium distribution on a timescale much faster than that of the reaction process. This allows the use of statistical thermodynamics. This assumption has been shown to be valid for very large systems in which there is enough anharmonic coupling between the systems various modes to redistribute the energy (e.g. Rice, 1980).

The jump falls into a particular class of reactions, the unimolecular reactions (e.g. Gilbert and Smith, 1990). Such reactions involve a rearrangement of a system of atoms, which ensures that there are the same number of degrees of freedom in both

reactant and transition state. For chemical reactions, the energy barrier is due to the breaking of chemical bonds, but for jumps, the energy barrier is due to straining components of the empirical potential. The rate coefficient for the jump is obtained from the TST formula, which is

$$k = \frac{k_B T}{h} \frac{Q^+}{Q} \exp\left(\frac{-E_0}{k_B T}\right) \tag{4.12}$$

where Q^+ and Q are the partition functions of transition state and reactant respectively, and E_0 is the difference in energy between reactant and transition state minima. It can be seen that such a formula requires no details of the dynamics of the jump. It only needs details of the potential energy surface for the reactant and transition state. The product state that the system moves to is irrelevant.

The number of degrees of freedom that are allowed to vary during the jump has been found to be important. The first application of TST to amorphous polymers by Gusev *et al*. (1993) allowed only the three *x*, *y* and *z* penetrant degrees of freedom to vary, leaving the polymer fixed. While *D*'s obtained for very small penetrants such as He compared reasonably with experiment, as the penetrants are nearly as small as the necks connecting cavities, *D*'s for larger penetrants such as O_2 were orders of magnitude smaller than experiment, as these larger penetrants must be significantly squashed to fit through the same necks. In order to give the polymer some flexibility, Gusev and Suter (1993) built in elastic thermal motion into the polymer during the stochastic simulations (Appendix B). Short MD runs were used to characterise and quantify these motions. *D*'s obtained agreed with experiment within an order of magnitude. To find the lowest energy path for a penetrant moving between two cavities, Greenfield and Theodorou (1993-95a,b) decided to allow polymer degrees of freedom to be explicitly included in the TST calculation, thus allowing the polymer to assist in forming a larger neck for the penetrant to squeeze through, relieving penetrant-polymer interactions. It is their work that will be used to assist in modelling diffusion. Their method is discussed in Section 4.4.

A dynamic correction factor can be used to correct for barrier recrossings (e.g. June *et al.*, 1991). It a number of order unity and lies between zero and one. It is found

by doing a short-time MD simulation of trajectories placed at the transition state and seeing whether they go into reactant or product minima. For large polyatomic systems it is believed (Miller, 1982) to be close to one, and is probably unnecessary to be calculated for order of magnitude estimates.

After locating reactant minima and transition state for all jumps and calculating their rate coefficients as well as how far the jumps go, as will be discussed in Section 4.4, a stochastic simulation can be performed to produce a macroscopic D (e.g. June *et al.*, 1991) (Appendix B). The advantage of stochastic simulations is that very long times can now be simulated, up to 1 μs (Gusev *et al*., 1993), since the basic time unit is now of order 1 ps rather than 1 fs as for MD. Yet these simulations still have their problems. This method does work for crystalline systems such as zeolites. However, for amorphous polymers, in which there are an extremely large distribution of jumps, the simulation box has to be large enough so that there are enough jumps available for penetrants to follow random paths and thus exhibit true Fickian diffusion. If the box is too small, false Fickian diffusion is observed, since the use of periodic boundary conditions enforces an artificial crystallinity on the polymer. It has been found (Gusev *et al*., 1993) that when penetrants on average have diffused the length of the box, a definite linear relationship between $<(r(t)-r(0))^2>$ and t sets in steeper than the relationship at shorter times, suggesting that D's obtained are too large. The box should be large enough so that there is no change in this relationship when penetrants have diffused the length of box.

4.4 Greenfield and Theodorou's TST Calculations

The system that Greenfield and Theodorou (1993-95a,b) looked at is glassy atactic polypropylene at 233 K. Polypropylene was chosen because it is a simple polymer with well-known potential interactions. It is chosen to be atactic, as this ensures that the polymer will be amorphous and not crystalline. The temperature was selected to make the polymer glassy. An empirical force field was used. A polymer matrix consisting of three polymer chains, each of 50 monomer units, was generated by the rotational isomeric state model modified to allow for non-bonded interactions, (Theodorou and Suter, 1985) then energy minimised by molecular mechanics. NPT

Monte Carlo moves were used to equilibrate the structures. One methane penetrant was considered. The united atoms approximation is used for methane and methyl groups. As well as the penetrants x, y and z degrees of freedom, torsion and bond angles associated with polymer atoms in a sphere of radius about 9 Å surrounding the penetrant were considered flexible. There are about f = 350 of these. As the penetrant moved, this set was continually updated so that it always surrounded the penetrant. All other degrees of freedom (N - f of them, with N being the total number of degrees of freedom) including all bond stretches were considered infinitely stiff (e.g. Go and Scheraga, 1976).

In order to find reactant cavities and connecting transition state necks, a geometric analysis of volume unoccupied by the polymer was performed (Greenfield and Theodorou, 1993). This eliminates large parts of the potential energy surface in which to search for true minima and transition states. Having to search the whole potential energy surface for them would prove a large waste of computer time and would probably be intractable.

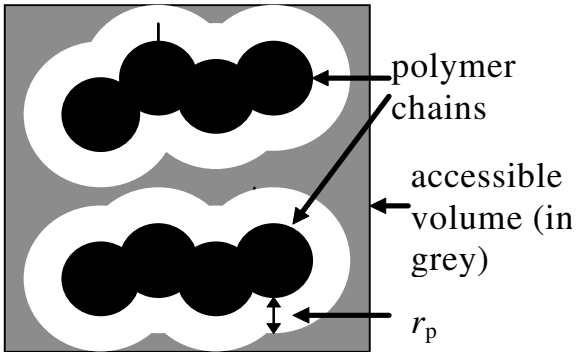

Figure 4.3: Illustration of regions of accessible volume for a penetrant with hard sphere radius r_p.

In order to talk about volume of the unoccupied volume, polymer and penetrant are treated as hard spheres with radii, r_p, given by $r_p = 2^{1/6}(\sigma/2)$, where σ is the Lennard-Jones diameter of the particular atom. Accessible volume for a penetrant of radius r_p is defined as volume in the polymer matrix traced out by the penetrant's centre for all the regions in which the penetrant can fit. In other words, as seen in Figure 4.3, if the radius of the polymer atoms is increased by r_p, the space left over is termed accessible volume. Unoccupied volume is just accessible volume for a penetrant with radius 0 Å. Greenfield and Theodorou used the method of Delaunay tessellation for volume calculations (Tanemura *et al.*, 1983), in which space is broken up into tetrahedra

with vertices at the polymer atoms. Accessible volume is then found by "clustering" these tetrahedra together. The accessible volume clusters they obtained are shown in Figure 4.4 for various penetrant radii. Naturally, there is less accessible volume for larger penetrants. The clusters for r_p = 2.09 Å corresponds to accessible volume for methane. Possible reactant and product cavities are not restricted to these structures, since polymer rearrangement and partial squashing of the penetrant, not considered in this hard sphere treatment, would allow methane molecules to fit into smaller cavities.

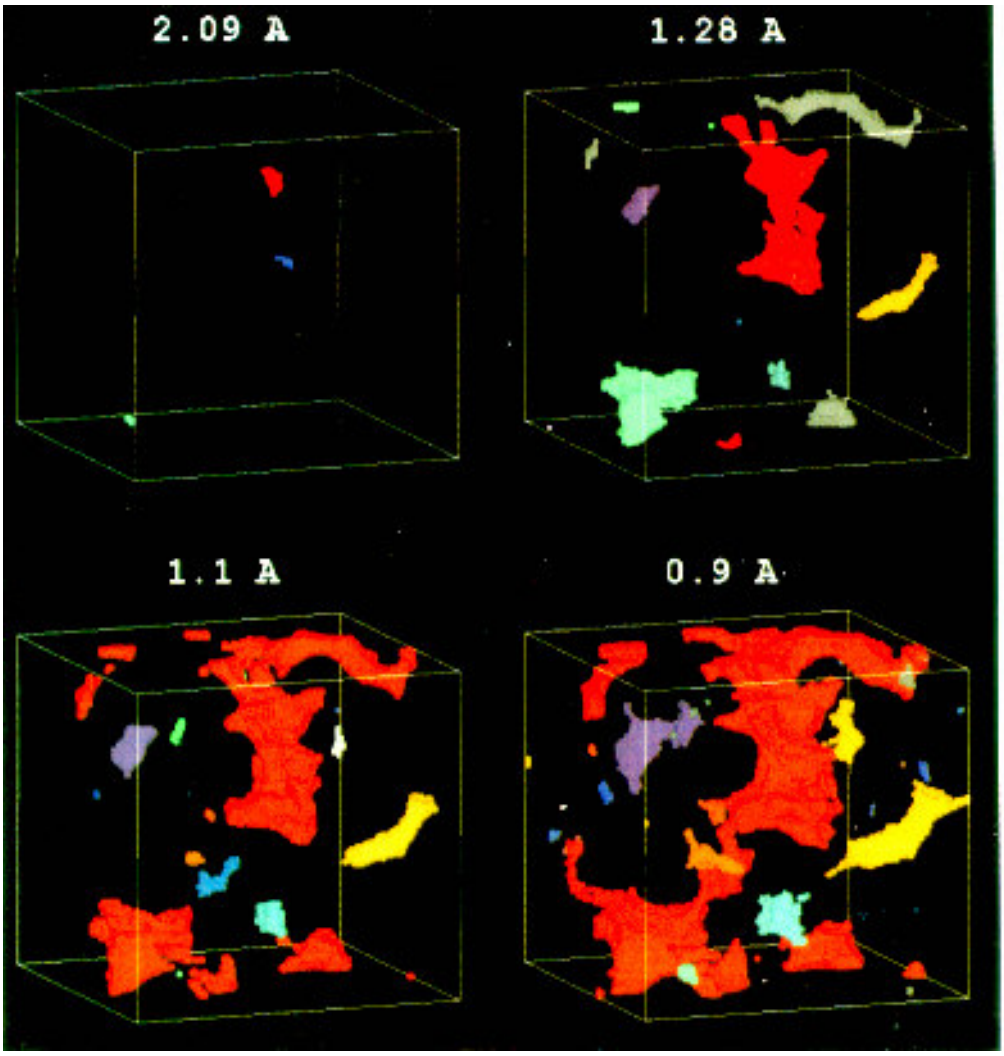

Figure 4.4: Greenfield and Theodorou's accessible volume clusters for penetrants of various radii (numbers shown). The shades are used to distinguish separate clusters.

Therefore possible reactant and product cavities are taken as clusters for r_p = 1.3 Å. Possible necks connecting them are taken from the accessible volume clusters for r_p = 0.7 Å. These clusters are shown in Figure 4.4. The details of evaluating k by the TST formula (Eq. 4.12) are given in Appendix C. Here is a quick summary.

After locating the reactant minimum and transition state accurately, the harmonic approximation is made to the potential energy surface at both reactant and transition state. This allows a normal mode analysis (Vineyard, 1957) to be performed, giving the normal modes and their frequencies at reactant and transition state. The reactant partition function is given by a product of vibrational partition functions

$$Q = \prod_{i=1}^{f} \left(1 - \exp\left(\frac{-h\upsilon_i}{k_B T} \right) \right)^{-1} . \qquad (4.13)$$

The formulae for the transition state partition function is the same, except that there are f-1 degrees of freedom (the reaction coordinate is not included).

The jump length is the displacement between reactant and product minima. However, reactant and product cavities consist of many minima separated by energy barriers small relative to $k_B T$, allowing penetrants ready access to the whole cavity. Thus the effective jump length is the displacement between the centres of reactant and product cavities. This modification was found not to make too much difference.

Greenfield and Theodorou are currently yet to complete calculations, so a full set of results is not available. However the details of the jumps, both forward and backward, through eight necks have been provided to us and are summarised in Table 5.1. It can be seen that rate coefficients, k, vary from 10^1 - 10^8 s^{-1}, energy differences, E_0, from 11 - 45 kJ mol^{-1}, and jump lengths, l, from 3 - 8 Å. These results are used in the development of a model to describe small molecule diffusion, which is discussed in Chapter 5.

Chapter 5

Development of a Model for Diffusion

5.1 The Jump

In order to obtain a penetrant diffusion coefficient, the penetrant's extremely complex motion in the polymer structure has to be simplified to motions that can be

characterised. Of these motions, of most importance is the bottleneck processes that will control the overall motion. In glassy systems, the jump clearly observed in MD simulations (Takeuchi, 1990b) is such a process. All other motion, except on very short time scales, is irrelevant to diffusion. There are no other competing diffusion mechanisms such as unoccupied volume redistributions sweeping along penetrants as in rubbery polymers, as the polymer matrix and cavities are mostly fixed in space, apart from a few fluctuations. It is assumed here explicitly that penetrants, while trapped in cavities, are unable to move a net displacement within the cavity which is significant with respect to the jump length. This might not be valid for very small penetrants, which see the cavities as quite large. The rate-determining step of the jump is *not* the time for the penetrant to jump from one cavity to another cavity, a process taking of the order 1 ps (Takeuchi, 1990b). It is in fact the time it takes while the penetrant is rattling around in the cavity for the polymer atoms to open up and form a neck, a process of the order at least 100 ps (Takeuchi, 1990b), extending up to at least 1 ns for some jumps (Tamai *et al*., 1994).

Thus the method of finding how fast penetrants diffuse reduces to calculating how fast all these jumps occur and how far they go. Transition state theory (for example, Gilbert and Smith, 1990) can be used to give the rate of jumping, k, by the TST formula, Eq. 4.12, given that models to predict E_0 and Q^+/Q can be provided. A third model to predict the jump length, l, for each jump is also required. Greenfield and Theodorou's simulations using TST (Greenfield and Theodorou, 1995b) show that there is a wide distribution of jumps, with rate coefficients varying from 10^{-1} to 10^{9} s^{-1}. Now even if one had a theory that was able to predict E_0, Q^+/Q and l for all these different jumps, there would still be the problem of putting all the jumps together as in the real polymer structure. Such a feat would require a knowledge of the distribution of jumps and correlation between successive jumps. Obtaining a macroscopic D is discussed in Chapter 6.

In order to get a model to predict D's, what is postulated is that an "average", "rate-determining" type of jump can be found. Penetrants, when they diffuse, then can only execute this jump. Models are then provided for the E_0, Q^+/Q and l of this jump. It is assumed that penetrants will execute this jump in a random manner, so that they

follow random walks. By stochastic theory (Chandrasekhar, 1943), the diffusion coefficient is then given by

$$D = \tfrac{1}{6} k l^2 . \qquad (5.1)$$

The idea behind this particular jump is the following. For a penetrant starting in any reactant cavity to diffuse a certain length scale, it must execute a certain number of jumps. Each sequence will have a slowest jump. If the penetrant is to now diffuse over larger length scales, each sequence will usually, but not always, have to include some slower jumps. There will be a point where enough jumps have been included for the penetrant to be able to percolate the entire polymer structure without the addition of more jumps. The sequence with the fastest "slowest jump" is assumed to form the fastest percolating network of jumps. The slowest jump in this fastest sequence is taken as this average, rate-determining jump for the model. Therefore, if penetrant diffusion is to proceed over a Fickian length scale, the penetrant will have to execute a jump at least as slow as this particular jump. The model to be discussed chooses parameters for this jump to capture this idea.

How valid is it to make this approximation? It effectively means that all jumps occur with the rate and jump length of this average, rate-determining jump. A full rate analysis has not been performed to determine if the above-mentioned jump to be modelled can be taken as the hypothetical jump, which, executed stochastically, gives the correct macroscopic D. The solution to such a rate problem may be in the literature, but is unknown to us. The assumption is that average jump assumption holds. The reason why the D is taken from the slowest jump and not the average of all the jumps in this fastest sequence is based on a timescale argument. Qualitatively, the faster jumps are effectively slowed down, since their reverse jumps will also be as likely to occur, roughly speaking, inhibiting diffusion. The slowest jumps, being rare, are likely to occur in isolated instances, implying that they are the critical jumps to net penetrant displacement.

What remains now is to define the reactant state and transition state and provide models of E_0, Q^+/Q and l for this average jump, giving a rate coefficient by TST, from which a diffusion coefficient can be obtained by stochastic theory. The simulations of

Greenfield and Theodorou (1993-95a,b) are used extensively in this modelling to indicate the important aspects of the mechanism and assist in making assumptions. Any mention of "the simulations" henceforth refers to their work. As a starting point for the analysis, they provided us with polymer structures for reactant, transition state and product polymer configurations and the key jump parameters for eight jumps taken from a particular polymer microstructure. Unless otherwise specified, all subsequent analysis of their data was done as These eight jumps were chosen at random and were meant to represent a typical collection of jumps in the polymer microstructure. Of course there are not enough jumps to ascertain various quantities on a statistical basis. Rather, it is hoped that eight are enough to show what features of the jumps are important. The key jump parameters are shown in Table 5.1.

Table 5.1: Parameters for forward and backward jumps of the eight jumps from Greenfield and Theodorou (1995b). E_{popo} is the energy for the polymer to form a neck, and E_{pepo} is the energy for penetrant to squeeze through the neck (discussed later).

jump number	E_0/kJ mol^{-1}	E_{popo}/kJ mol^{-1}	E_{pepo}/kJ mol^{-1}	Q^+/Q	k / 10^6 s^{-1}	l / Å
1 forward	18.1	6.2	11.9	0.18	77	7.6
1 backward	23.5	6.3	17.2	0.36	9.3	
2 forward	11.3	9.6	1.7	0.024	336	5.9
2 backward	19.1	10.7	8.4	0.20	52	
3 forward	32.7	26.6	6.1	0.12	0.0027	5.4
3 backward	24.3	18.5	5.7	0.79	14	
4 forward	41.0	26.5	14.3	0.0056	2×10^{-5}	7.6
4 backward	45.3	25.3	20.0	0.0074	3×10^{-5}	
5 forward	19.8	8.3	11.5	0.0020	0.37	6.8
5 backward	12.8	6.1	6.7	0.0001	0.63	
6 forward	27.1	21.7	5.4	0.050	0.20	3.2
6 backward	16.6	12.5	4.1	0.13	115	
7 forward	19.4	19.1	0.3	0.050	13	3.0
7 backward	14.7	14.0	0.3	0.024	58	
8 forward	22.6	13.9	8.8	0.076	3.0	4.6
8 backward	33.3	22.0	11.4	0.070	0.011	

5.2 Model for *l* for the Average Jump

The jump length is the displacement of the penetrant in jumping from one cavity to another cavity. The simulations produce *l*'s of 3 - 8 Å. Intuitively, when a penetrant jumps from one cavity to another cavity, it will have jumped through a neck past some part of the polymer chain. Treating polymer atoms surrounding the penetrant as hard spheres with radius $\sigma/2$ (σ is the Lennard-Jones diameter), Table 5.2, calculated from

Greenfield and Theodorou's data, shows the four polymer atoms whose surfaces, not their centres, are closest to the penetrant in the transition state for each jump.

Table 5.2: The types of polymer atoms closest to the penetrant in the transition state for each jump, together with the distances from the surfaces of these polymer atoms to penetrant centres, and the non-bonded energies between penetrant and polymer atoms (Me = methyl, H = hydrogen, C = carbon).

jump number	atom type	distance from polymer atom surface to penetrant centre / Å	non-bonded energy between penetrant and polymer atom /kJ mol^{-1}
1	Me	1.69	2.13
	Me	1.70	2.05
	Me	1.84	0.45
	Me	1.86	0.28
2	Me	1.73	1.51
	Me	1.79	0.93
	Me	1.79	0.90
	H	1.95	-0.16
3	Me	1.59	4.19
	H	1.62	3.68
	C	1.71	1.47
	H	1.71	1.78
4	C	1.57	3.63
	H	1.60	4.01
	H	1.66	2.83
	C	1.69	1.69
5	Me	1.72	1.74
	Me	1.76	1.24
	Me	1.76	1.24
	Me	1.81	0.75
6	H	1.66	2.84
	H	1.70	2.01
	H	1.74	1.44
	H	1.75	1.33
7	Me	1.70	2.01
	Me	1.73	1.53
	H	1.83	0.48
	Me	1.85	0.38
8	Me	1.56	4.86
	Me	1.68	2.22
	H	1.72	1.74
	Me	1.79	0.88

It can be seen that jumps most commonly go past methyl atoms, followed by hydrogens and then carbons. This suggests taking average jumps past methyl atoms. Jumps past carbon atoms (numbers 3,4) can be discounted since they are very high in energy, as seen in Table 5.1, so it is reasonable to assume that they will not form part of the fastest percolating network. Jumps 1,2,5,7 and 8 seem to be the most common type of jump observed. These jumps have mostly methyls and a few hydrogens surrounding the necks. Thus the assumption is made that the average jump goes through a neck

whose thickness is the Lennard-Jones diameter of a methyl atom, namely 3.56 Å. Since the jump length goes from the centre of the penetrant in the reactant cavity to that in the product cavity, the thickness of the penetrant also needs to be included in the jump length, as can be seen in Figure 5.1. The penetrant is assumed to travel a negligible distance within a cavity.

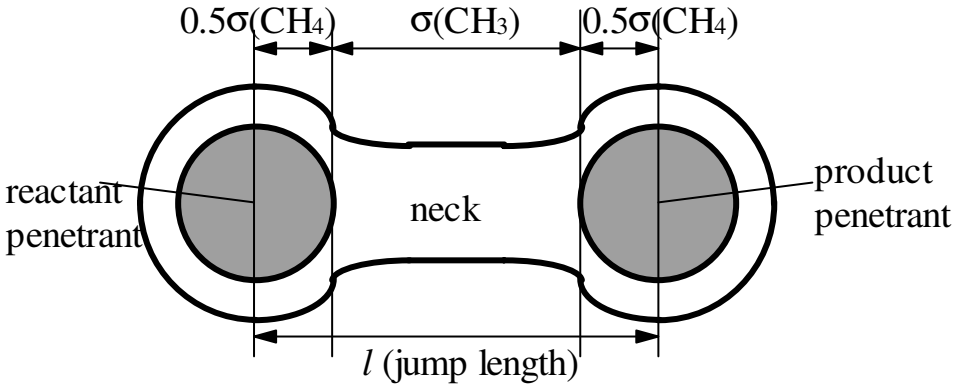

Figure 5.1: Sketch showing how the jump length, *l*, is constructed, given the assumed geometry of the cavities and neck.

For the average jump, taking the necessary Lennard-Jones parameters from Table 5.3,

$$\begin{aligned} l &= \tfrac{1}{2}\sigma(CH_4) + \sigma(CH_3) + \tfrac{1}{2}\sigma(CH_4) \\ &= \tfrac{1}{2}(3.82) + 3.56 + \tfrac{1}{2}(3.82) \\ &\approx 7 \text{ Å} \end{aligned} \qquad (5.2)$$

Table 5.3: Lennard-Jones ε and σ for methyl atoms and methane penetrants.

atom type	ε / kJ mol^{-1}	σ / Å
methyl	0.580	3.56
methane	1.23	3.82

This lies in the upper range of *l* from the simulations (3 - 8 Å). If the jump was past hydrogen atoms, $l \approx 6$ Å. There are a number of other factors not considered in the model that could influence *l*. They have been ignored either because they are assumed to be small, or they are difficult to quantify. Firstly, the penetrant might be able to move some distance within the cavity, but this will be assumed to be negligible. This assumption could break down for very small penetrants, or for very large cavities. Secondly, the model assumes that the cavities remain relatively fixed in space during the course of the jump. It might happen that once the penetrant has squeezed past the neck atoms into the product cavity, the neck atoms are pushed into the reactant cavity

where there is now empty space. Thus, the penetrant has not jumped past the whole width of the neck atoms but only a small part of them, making l less. This could be especially important for penetrants larger than typical cavity sizes, since the product cavity must expand for such a penetrant to fit, and the easiest way to do this is likely to involve polymer filling up the reactant cavity. The simulations do suggest a trend that if the penetrant in either the reactant or product cavity is already partially squashed (that is, some non-bonded interactions between penetrant and polymer atoms are large and positive), then the jump length is shorter. Thirdly, the assumed geometry of the atoms is rather crude. Given that there already is a pre-existing neck and the spherical nature of the arrangement of neck atoms, the distance between reactant and product atoms might be less than the diameter of the neck atoms, as shown in Figure 5.2.

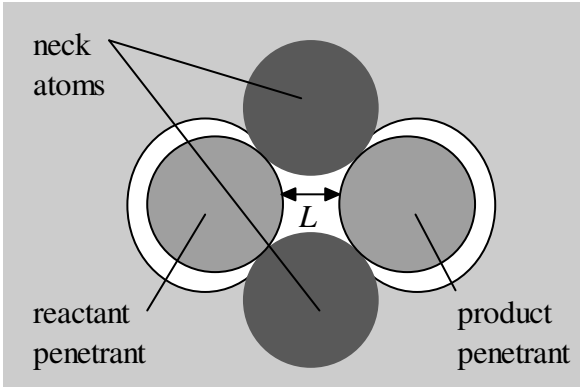

Figure 5.2: A possible neck structure such that L is less than the diameter of the neck atoms.

Such a situation would also be more likely when the penetrant is squashed in a reactant or product cavity, providing another reason for shorter l's. The assumption of this model is that penetrants are not squashed in reactant or product cavities, and so it is reasonable to assume that, on average, penetrants jump past the whole width of a methyl atom.

5.3 Model for E_0 for the Average Jump

E_0 is the difference in energy on the system potential energy surface between reactant and transition state. Since an empirical force field is used in the simulations, the components of E_0 are harmonic bends and stretches, three-fold torsional potentials and non-bonded Lennard-Jones potentials. To find E_0, either key components that change significantly need to be picked out, or, if many components change, a formulation that averages these changes is required.

E_{popo} is defined as the energy for the polymer to form a neck, so named because it consists of changes in energy contributions involving just polymer atoms, namely bends, torsions and non-bonded Lennard-Jones interactions between polymer atoms. E_{pepo} is defined as the remainder, being the energy for the penetrant to squeeze through the neck, which is due to changes in non-bonded Lennard-Jones interactions between the penetrant and polymer atoms. The simulations, which calculate the minimum energy path, show that both contributions are important, as seen in Table 5.1, with E_{popo} on average about two-thirds of E_0 and E_{pepo} about one-third. Figure 5.3, taken from the simulations shows how these contributions vary along the reaction coordinate for a jump.

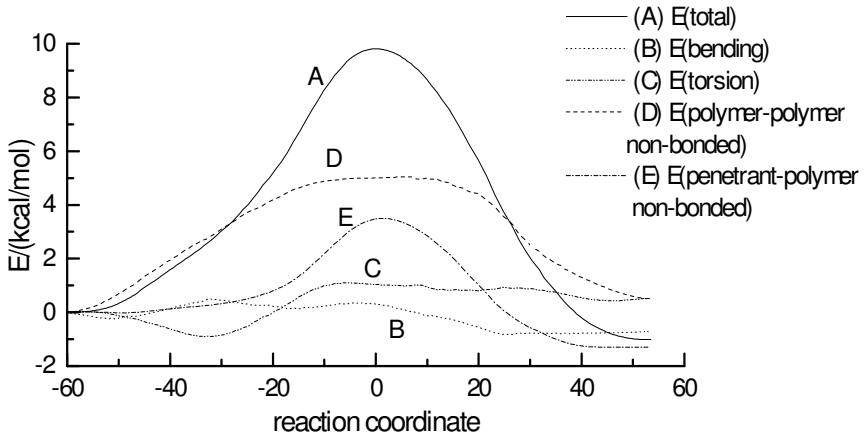

Figure 5.3: The energy profile along the reaction coordinate for jump number 4. Shown also are the changes in the individual energy contributions (bends, torsions, polymer-polymer non-bonded, penetrant-polymer non-bonded). Note that the energy is in kcal/mol.

It is important to note the competing nature of E_{popo} and E_{pepo}. It is the size of the neck to be formed that determines their relative contributions. In order to parametrise these energy contributions by the size of the neck, the model assumes that the neck can be approximated by a cylinder with radius r and length L, as seen in Figure 5.4.

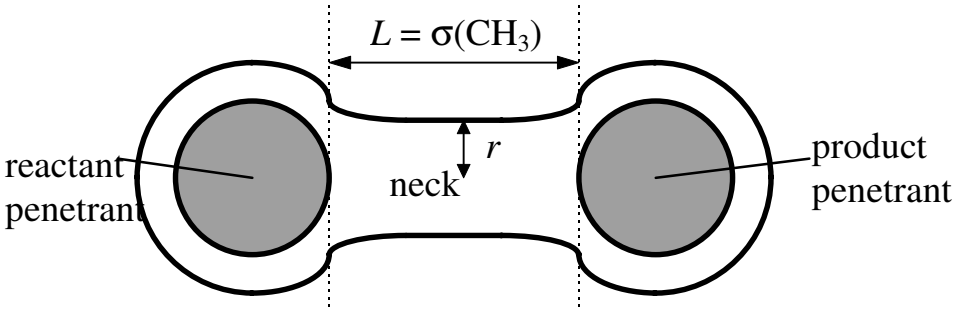

Figure 5.4: Diagram showing the assumed structure of the neck connecting reactant and product cavities as a cylinder, with radius, r, and length $\sigma(CH_3)$.

Treating polymer neck atoms as hard spheres with Lennard-Jones diameters, the radius of the neck, r, is the radius of the largest cylinder that can be fitted in the neck. Since the average jump was assumed to go past a methyl atom, as discussed in section 5.2, the length of the cylinder is taken as the Lennard-Jones diameter of a methyl atom.

The following two potential functions are set up. $V_{popo}(r)$ is defined as the energy required for a polymer to form a neck of radius r. A qualitative sketch of it is shown in Figure 5.5.

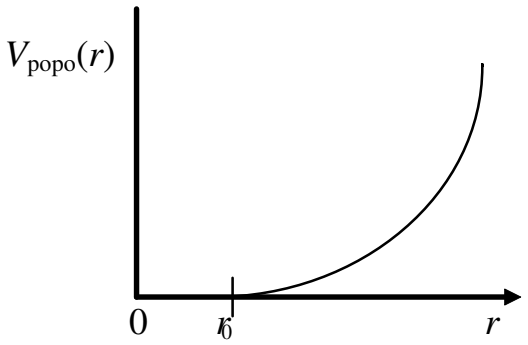

Figure 5.5: Qualitative sketch of $V_{popo}(r)$, the energy required to form a neck of radius r. r_0 is the radius of the pre-existing neck in the reactant state.

r_0 is the radius of the pre-existing neck in the reactant state. If a neck of radius $r < r_0$ needs to be formed, no energy is required, since a large enough neck is already present. The larger the neck formed, the more energy it takes to do that.

Now a quantitative functional form for $V_{popo}(r)$ is put forward. It will be shown that forming a neck is a cooperative process involving small contributions from many atoms to $V_{popo}(r)$. The model used is going to treat these contributions in an average sort of way. Here are reasons why it is suspected to be such a cooperative process, and not a short-range process such as a few methyl atoms bending out of the way. Firstly, when Greenfield and Theodorou initially did their simulations, they allowed a smaller sphere of polymer atoms around the penetrant to be flexible. The result was that E_0's obtained were much higher than those obtained when they allowed many more polymer atoms further from the neck to move, which they later did. They believe that they currently allow enough polymer atoms to move, with E_0 seeming to converge. However, a proper test of this by allowing even more polymer atoms to move is not possible given the

computational restrictions. It does suggest that there are at least as many polymer atoms participating in forming the neck as the number allowed flexible in Greenfield and Theodorou's first treatment.

Secondly, in virtually every jump from the simulations, polymer-polymer non-bonded interactions made a large positive contribution to E_{popo}, as can be seen in Figure 5.3. Torsional and bending energy contributions fluctuated about zero, sometimes quite large in magnitude, but there was no consistent trend in their behaviour. This suggests that forming the neck is not the result of a few local bends or torsions. As an example, with typical bond angle stretching force constants of 500 kJ mol^{-1}, a bend of 10° costs roughly 5 kJ mol^{-1}. A few of these combined with a few other associated contributions would soon give an energy greater that E_0. Torsional contributions are likely to small, firstly because their force constants are small (of the order 10 kJ mol^{-1}), and secondly because any torsional rotations will be small due to steric reasons.

The third reason that neck-forming involves many atoms is that polymer atoms are connected together by bonds so they will tend to move together rather than having one moving by itself.

In the spirit of the average jump, to simplify the local polymer structure surrounding the neck, the model assumes that this structure can be averaged out and treated as an isotropic continuum with thermodynamic properties of the bulk. In forming the neck, the above three reasons suggest that enough of the polymer is involved such that this approximation can be made. The particular property of the bulk that is used is the isothermal compressibility, κ, which quantifies how the volume of a material changes in response to a pressure change at constant temperature, as shown in Eq. 5.3.

$$\kappa = -\frac{1}{v}\left(\frac{\partial v}{\partial p}\right)_T \tag{5.3}$$

Now the work, W, to create a volume, v, against a given pressure, p, provided by the polymer, is given by

$$W = \int_{v_0}^{v} p dv' \tag{5.4}$$

where v_0 is the original volume, and v' is the integration variable of volume. Using the simplest level of treatment, since the change in volume of the polymer will be small, the pressure similarly will hardly vary and can thus be approximated by a constant value. It is assumed that over this small range of volume change, the pressure is inversely proportional to the volume of the polymer (ideal gas approximation), giving a pressure of $1/\kappa$ (substitute v = (constant)/p into Eq. 5.3). This is a rather approximate treatment, but given time constraints, a more sophisticated expression for the relationship between pressure and volume has not yet been found (see Section 6.1). Treating the neck as a cylinder, the volume change is a concentric expansion of this neck from old radius r_0 to new radius r. So when $r > r_0$, $V_{popo}(r)$ is given by

$$\begin{aligned} V_{popo}(r) &= 10^{-3} N_A \int_{v_0}^{v} \frac{1}{\kappa} dv'(r) \\ &= \frac{10^{-3} N_A \pi L (r^2 - r_0^2)}{\kappa} \end{aligned} \tag{5.5}$$

The factor of $10^{-3}N_A$ is introduced to convert this to kJ mol^{-1}. As mentioned before, if $r < r_0$, then $V_{popo}(r)$ equals zero. It would be interesting to see from the simulations if the energy to form a neck shows such a dependence on r_0 for each individual jump. There are more sophisticated treatments of the pressure, but these are discussed in Chapter 6.

The parameters in this equation need to be stated. L is taken as the Lennard-Jones diameter of a methyl atom (Figure 5.5), which is 3.56 Å (Table 5.3). While experimental data could not be found for κ of atactic polypropylene at 233 K, it has been calculated from the simulated structures (Boone, 1995) to be 3.0×10^{-10} Pa^{-1}. For r_0, Greenfield and Theodorou's simulations (1993) showed that onset of percolation in the polymer structure occurs for penetrants of radius 1.1 Å. Thus there is an accessible volume cluster for such a penetrant, the so called infinite cluster, that stretches across the entire simulation cube. They treat polymer and penetrant atoms as having hard sphere radii of $1/2(2^{1/6}\sigma)$. This model requires the percolation radius of a penetrant when polymer and penetrant atoms are treated as having radii of $1/2(\sigma)$. The difference in radius, Δr, between a methyl atom of radius $1/2(2^{1/6}\sigma)$ and one of radius $1/2(\sigma)$ is

$$\Delta r = \tfrac{1}{2}\sigma\left(2^{1/6} - 1\right) \approx 0.2 \text{ Å}. \tag{5.6}$$

Figure 5.6 illustrates the modification, Δr, to the percolating penetrant's radius.

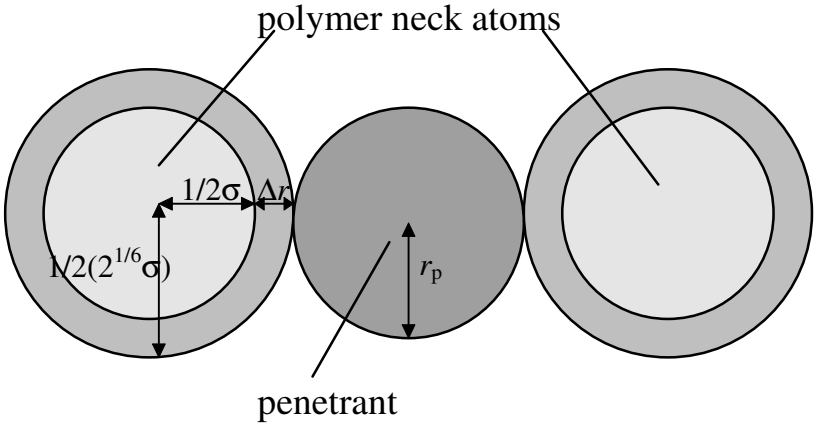

Figure 5.6: Illustration of how the percolation radius of the penetrant is increased by Δr when considering polymer atoms as having radius of 1/2(σ).

This suggests that a penetrant of radius 1.1 + 0.2 = 1.3 Å can percolate the structure, where polymer and penetrant atoms are now treated as hard spheres with radius 1/2(σ). Hence, r_0 is taken as 1.3 Å.

A few points need to made about this choice of r_0 for the average jump. By taking r_0 as the largest possible percolation radius, and assuming that the energy for the jump depends only on how wide the pre-existing reactant neck was, this makes the average jump the slowest jump in a percolating network. It could be argued that r_0 should be larger, since all other jumps in the percolating pathway will be faster. On the other hand, r_0 could be taken as smaller, since the percolation radius seen in the simulations across a 23 Å box might have artificially converged on the small simulation length scale. In other words, such a penetrant might not percolate a larger box.

The second potential function needed is $V_{\text{pepo}}(r)$. It is the energy required for the penetrant to push through a neck with a given radius, r. A qualitative sketch of it is shown in Figure 5.7.

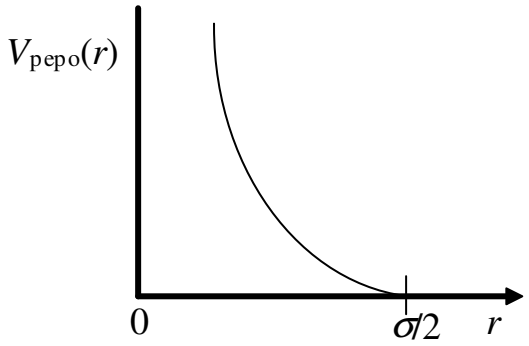

Figure 5.7: Qualitative sketch of $V_{pepo}(r)$, the energy for the penetrant to push through the neck. σ is approximately the Lennard-Jones diameter of the penetrant, σ_p.

The larger the neck becomes, the less the penetrant has to be squashed, making $V_{pepo}(r)$ smaller, until the neck is so wide that the penetrant does not have to be squashed at all, at which point, $V_{pepo}(r)$ equals zero.

Here is the functional form of $V_{pepo}(r)$ of the model. The simulations show that the non-bonded interactions between penetrant and the closest polymer atoms in the reactant cavity can range from slightly negative (~0.7 kJ mol^{-1}) to zero right through to the odd few being reasonably positive (~2 kJ mol^{-1}). However, in the transition state, as can be seen in Table 5.2, the penetrant has large repulsive interactions with three to four polymer neck atoms, most of which are methyls. The model assumes that the neck for the average jump is made up of three methyl atoms arranged symmetrically, as shown in Figure 5.8.

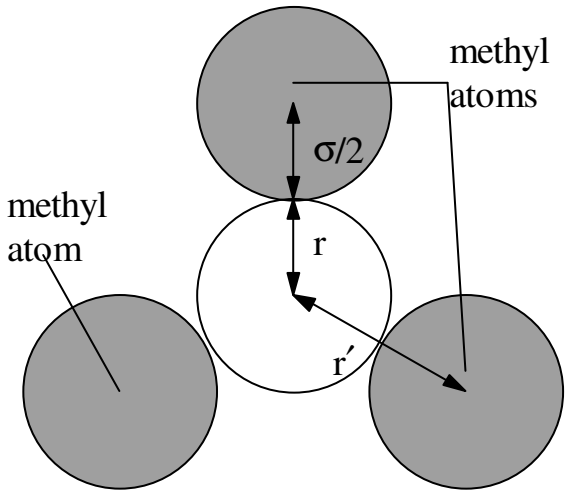

Figure 5.8: Assumed arrangement of neck atoms, which are three methyls. This is a cross-section of the neck.

The assumption is then made that the difference in penetrant-polymer non-bonded energy in taking the penetrant from reactant to the neck in the transition state is due to the repulsive interactions between the penetrant and these three methyl atoms. This assumption will only hold when the neck is less than the Lennard-Jones diameter of the penetrant. Otherwise, these repulsion interactions will be small, making other energy changes such as those in attractive energy interactions important. Thus $V_{\text{pepo}}(r)$ is taken as three Lennard-Jones potentials, one between each methyl and the penetrant, as shown,

$$V_{pepo}(r) = 3\left[4\varepsilon\left(\left(\frac{\sigma}{r'}\right)^{12} - \left(\frac{\sigma}{r'}\right)^{6}\right)\right] \tag{5.7}$$

where

$$r' = r + \tfrac{1}{2}\sigma(CH_3) \tag{5.8}$$

is the distance between methyl and penetrant atoms, as seen in Figure 5.8, and σ and ε are obtained using the standard mixing rules for Lennard-Jones interactions between different atoms (Eqs. 4.5, 4.6). The Lennard-Jones parameters for this interaction are in Table 5.3.

Overall, $V(r)$ is given by

$$V(r) = \frac{10^{-3} N_A \pi L}{\kappa}\left(r^2 - r_0^2\right) + 3\left[4\varepsilon\left(\left(\frac{\sigma}{r'}\right)^{12} - \left(\frac{\sigma}{r'}\right)^{6}\right)\right]. \tag{5.9}$$

It is plotted in Figure 5.9.

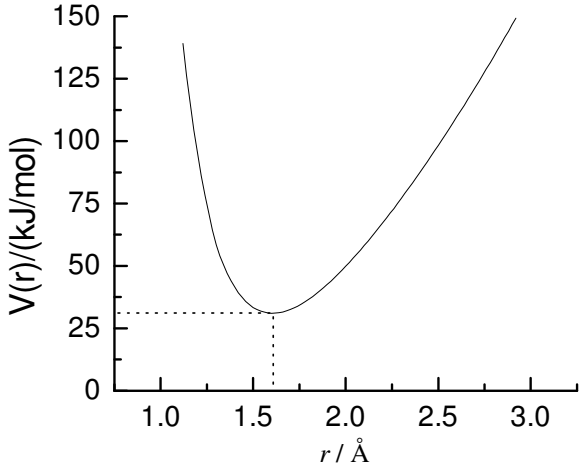

Figure 5.9: Graph of the function $V(r)$. The minimum of 31 kJ mol^{-1} is E_0, which occurs at r = 1.6 Å.

E_0 is given by the minimum value of this function, the transition state is situated at the top of the *lowest* energy path connecting two minima. The graph gives $E_0 = 31$ kJ mol^{-1}, with contributions of $E_{popo} = 19$ kJ mol^{-1} and $E_{pepo} = 12$ kJ mol^{-1}. The neck radius at this minimum is 1.6 Å. This can be compared with the simulations, which give $E_0 \sim 12$ - 40 kJ mol^{-1}.

An interesting plot to make is how E_0 varies with penetrant size. This can be achieved by varying σ, the Lennard-Jones diameter to values other than that of methane. For simplicity, ε is set to that of methane. The result is shown in Figure 5.10.

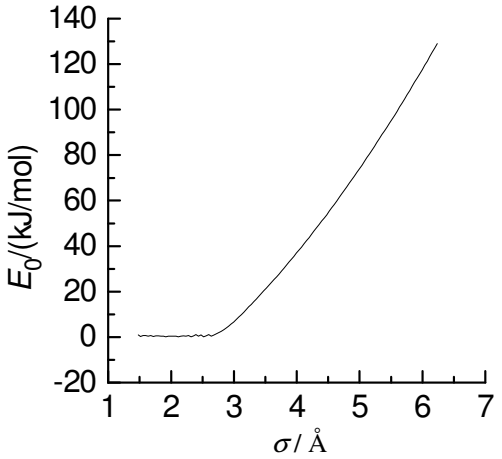

Figure 5.10: Graph of E_0 versus σ (Lennard-Jones diameter) as predicted by the model.

The result is a slightly steeper than quadratic dependence of E_0 on σ. Naturally, E_0 becomes zero for penetrants smaller than the pre-existing neck diameter of 2.6 Å. This behaviour is evident from equation 5.11. If one assumes that E_{pepo}, due to the steepness of $V_{pepo}(r)$, remains essentially constant when σ is varied a little, then consider just $V_{pepo}(r)$. Noting that the radius of the neck to be formed is roughly $\sigma/2$, substituting σ from Eq 4.5 into Eq. 5.5, one obtains

$$V_{popo} = \frac{10^{-3} N_A \pi L \left[\frac{1}{2} \left(\sigma(CH_3) + \sigma(penetrant) \right)^2 - r_0^2 \right]}{\kappa} \qquad (5.10)$$

which has a quadratic dependence on σ(penetrant).

5.4 Model for Q^+/Q for the Average Jump

Q^+/Q is the ratio of partition functions, Q^+ being the partition in the transition state and Q the partition function in the reactant state. Intuitively, the system will be

more constrained in the transition state, with more atoms being compressed against eachother and thus with less room to move. They will have higher frequency vibrations, which gives a larger partition function by the vibrational partition function formula (Eq. 4.13).

To evaluate a partition function, it is simpler if the overall motion of the system can be broken up into components such as vibrations, for which there are known partition function formulas. This model assumes that both Q^+ and Q can be broken up into three components each, one due to penetrant, q_{pe}, one due to polymer, q_{po}, and one due to the interaction between penetrant and polymer, q_{pepo}. So one can write

$$\frac{Q^+}{Q} = \frac{q_{pe}^+ q_{po}^+ q_{pepo}^+}{q_{pet} q_{po} q_{pepo}} \quad . \tag{5.11}$$

Since the penetrant is treated as a united atom, it has no internal degrees of freedom, and so

$$q_{pe}^+ = q_{pe} = 1 \tag{5.12}$$

To obtain penetrant-polymer partition functions, in each case the harmonic approximation is made to the potential. The neck is assumed to consist of 3 methyls, as in Figure 5.8. The simulations show that the most common type of polymer atoms around penetrants in reactant cavities are methyls as well, so 4 methyls tetrahedrally arranged are assumed to be these atoms. The force constant, λ, of the harmonic potential is given by the second derivative of the potential, taken to be n Lennard-Jones potentials (Eq. 5.13), where n is the number of methyl atoms.

$$\lambda = n \frac{4\varepsilon\sigma^6}{r'^8} \left[\frac{156\sigma^6}{r'^6} - 42 \right] \tag{5.13}$$

As defined in Section 5.3, r' is the distance between penetrant and polymer atoms. The frequencies of vibrations are obtained by the equation

$$\nu_i = \sqrt{\lambda_i} \,/\, 2\pi \,, \tag{5.14}$$

and then Eq. 4.13 gives partition functions. In the reactant state, the distance between atoms, r', is taken as the sum of Lennard-Jones radii of methane penetrant and methyl atom, which gives 3.69 Å. There are three such vibrations for the reactant. In the transition state, r' is taken as the sum of the Lennard-Jones methyl radius plus the neck

radius, obtained from the E_0 calculation, which gives 3.40 Å. There are only two vibrations for the transition state, since one degree of freedom is taken as the reaction coordinate. Figure 5.3 shows a plot of frequency versus $r^{\prime}$.

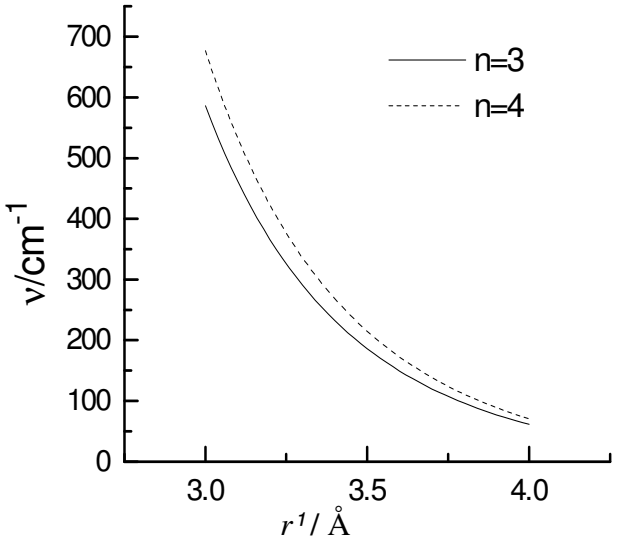

Figure 5.11: Plot of harmonic frequency, v, versus $r^{\prime}$, the distance between methane penetrant and polymer methyl atoms for n = 3 and 4 (n is the number of methyl atoms).

Thus

$$\frac{q^{+}_{pepo}}{q_{pepo}} = \frac{(1.3)^2}{(1.7)^3} = 0.34 \tag{5.14}$$

While $q^{+}_{\mathrm{po}} / q_{\mathrm{po}}$ is expected to be slightly less than 1 (see Section 6.4), since the polymer will be more constrained in the transition state, no way was found to quantify this. So the approximation is made that

$$\frac{q^{+}_{po}}{q_{po}} = 1. \tag{5.15}$$

Thus, combining all three components, the overall partition function is given by

$$\frac{Q^{+}}{Q} = 0.34 \tag{5.16}$$

In comparison, the simulations give $Q^{+}/Q \sim 10^{0}$ - 10^{-4} s^{-1}, as can be seen in Table 5.1.

5.4 Evaluation of a Diffusion Coefficient

The above estimated parameters Q^+/Q and E_0, by the TST formula (Eq. 4.12), give a rate coefficient, k, for the average jump of 1.9×10^5 s^{-1} (Greenfield and Theodorou's k's vary from 10^{-1} to 10^9 s^{-1}). By stochastic theory (Eq. 5.1) using the estimated jump length, a macroscopic D for the methane penetrant is obtained of 2×10^{-10} $cm^2 s^{-1}$ (10^{-10} - 10^{-9} $cm^2 s^{-1}$).

Table 5.4: The parameters predicted by the model, needed to estimate a diffusion coefficient.

l / Å	Q^+/Q	E_0 / kJ mol^{-1}
7	0.34	31

While no experimental data for methane in atactic polypropylene at 233 K could be found, a polymer similar in structure is poly(vinyl chloride) (PVC), since it has a chloride atom instead of a methyl atom. At 298 K it is glassy, and methane has a D of 1.3×10^{-9} cm^2 s^{-1} (Koros *et al.*, 1988). To make the comparison slightly more meaningful, D of methane predicted by the model at 298 K for the same polymer structure is 6×10^{-9} $cm^2 s^{-1}$, which is within order of magnitude agreement.

The temperature dependence of D predicted by the model is basically Arrhenius, with the pre-exponential T and Q^+/Q slowly varying with respect to temperature relative to the exponential. Such a prediction is supported by the experimentally measured D's in Figure 3.2 in the glassy region. One aspect of temperature dependence that the model has not taken into consideration is change in the polymer structure with temperature. Of course, the model is designed for glassy polymers, but even in these, the unoccupied volume fraction still decreases with temperature (e.g. Kovacs, 1958). How this affects the necks and cavities could be important, but is unknown.

Figure 5.12 shows how D is predicted to vary with penetrant size. It is also plotted at 298 K so that it can be compared with the experimental data of Koros *et al.* (1988) in PVC.

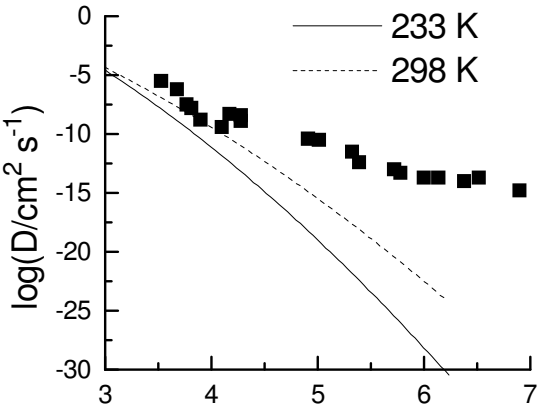

Figure 5.12: Prediction of the model of how D varies with penetrant Lennard-Jones diameter at T = 233 and 298 K. The points are experimental data for various penetrants in PVC (Koros *et al.*, 1988)

The agreement is reasonable for small penetrants ($\sigma < 4.5$ Å), but D predicted by the model drops away for larger penetrants. This could partly be explained by the fact that these larger penetrants were approximated by spheres. Such an approximation worsens with larger penetrants, which are more likely to be aspherical, with the smallest cross-sectional area having a diameter smaller than the average. Hence the experimental points could be shifted to the left. The question of whether the jump mechanism is still occurring as assumed in the model for these larger penetrants is unknown. Such large penetrants, being too large for the existing polymer cavities, could significantly disrupt the polymer structure, removing the distinction between cavities and necks. Jumps might still occur, but might only be partial jumps involving a slight shift of the penetrant. The penetrant might even follow some sort of "burrowing" motion, forcing apart polymer chains already partially opened up by the presence of this large penetrant. The details of these motions would have to be elucidated with MD simulations.

Chapter 6

Other Considerations in Modelling Diffusion

This chapter is intended to describe some of the possible extensions to the model described in Chapter 5. They are concerned with expected qualitative aspects of the model. Since they were not able to be properly quantified, none of them were able to be successfully incorporated into the model.

6.1 More Sophisticated Models for V_{popo}

A number of attempts are given here towards calculating the work done to expand a cylinder in a polymer, termed V_{popo}. The first assumes that pressure is related to volume by

$$p = -\frac{1}{\kappa}\ln\left(\frac{v}{v_0}\right) \tag{6.1}$$

which is derived by integrating volume with respect to pressure in the definition of isothermal compressibility (Eq. 5.3). The initial volume of polymer is v_0, for which the pressure is assumed to be zero. Substituting Eq. 6.1 into Eq 5.4 gives

$$\begin{aligned} V_{popo}(r) &= \frac{1}{\kappa}\left(v(r)\ln\left(\frac{v(r)}{v_0}\right) + (v_0 - v(r)) \right) \\ &\approx \frac{\left(v_0 - v(r)\right)^2}{2\kappa v_0} \end{aligned} \tag{6.2}$$

The problem with this approach is that it has an adjustable parameter, v_0, which cannot be predicted. Attempt to quantify it or make modifications to eliminate it were unsuccessful.

A second approach that has not been calculated yet is to treat the neck expansion the way a mechanical engineer would an expanding pipe by using the theory of elasticity (Tanner *et al.*, 1990; Zhang, 1994; Popov, 1990). Calculating the stress and strain tensors gives the strain energy density for the compressed polymer, which, integrated over the compressed polymer volume gives the energy to compress it (see Appendix D).

6.2 Modelling l, Q^+/Q and E_0 for Different Jumps

It was obvious from the simulations of Greenfield and Theodorou (1993-95a,b) that there is a wide distribution of jumps, as would be expected in an amorphous polymer. Rather than assuming that diffusive motion in a polymer can be chacterised by one single jump, motion involving many jumps ought to be considered. The first question that needs to be asked is, what makes jumps different, each with their particular l, Q^+/Q and E_0? What characteristics of a jump can be quantified and built into the model?

Jump lengths would vary for the following reasons. The jumps would be past different atoms. A cavity might be large enough such that a significant displacement might be possible within the cavity. The polymer chains might rearrange significantly, shifting the product cavity. These adjustments would require the identity of the neck atoms and the size of reactant and product cavities. However, given that the simulations did not find the range of l to be very large, the approximation of taking an average value would not be too inaccurate.

Variations in E_0 would be due to variations in $V_{\text{pepo}}(r)$ and $V_{\text{popo}}(r)$. Firstly, $V_{\text{pepo}}(r)$ would depend on the type of neck atoms, so the Lennard-Jones parameters would be adjusted accordingly. Furthermore, penetrants in reactant cavities might have slightly negative or positive non-bonded interactions with the closest polymer atoms, not zero as the model assumes. The variation of $V_{\text{popo}}(r)$, however, is expected to be more complicated. The radius of the pre-existing neck, r_0, would be a source of variation. However, perhaps of even more importance is how easily the polymer expands to form the neck. The polymer chains around one particular neck might be surrounded by much unoccupied volume into which they can easily move to form the neck. Thus $V_{\text{popo}}(r)$ in this case would be shallower than for necks surrounded by less unoccupied volume. This could be built in by allowing the local isothermal compressibility, κ, to vary locally. An attempt was made to do this using the isothermal compressibility equation

$$\rho k_B T \kappa - 1 = \rho \int_0^\infty 4\pi r^2 (g(r) - 1) dr \tag{6.3}$$

where ρ is the number density and $g(r)$ is the radial density distribution function. The $g(r)$ used was not averaged over many origins in the traditional sense but taken only about the point where the penetrant is when in the transition state (to avoid using the TST simulation data, the origin could be taken as the narrowest point of the neck instead). It is shown in Fig 6.1a.

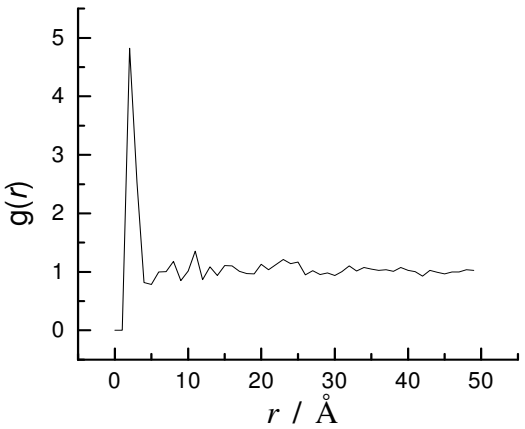

Figure 6.1a: The g(r) plot calculated for jump 8. jump 8. Note the noise even at large r.

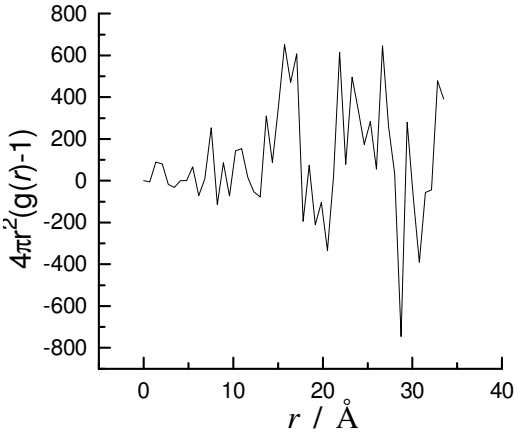

Figure 6.1b: $4\pi r^2(g(r)-1)$ plotted against r for The noise in g(r) , multiplied by r^2, gets amplifed.

However, the $g(r)$, being unaveraged and because it is taken over an array of periodic boxes, caused the integrand to diverge for large r (Fig, 6.1b), so this calculation was not possible. Another attempt involved measuring the amount of unoccupied volume surrounding the neck, from which a radial distribution function of unoccupied volume could be constructed. Variation in this for different jumps would similarly vary V_{popo} for each jump. However, the unoccupied volume program of Greenfield and Theodorou (1995b) was not able to be successfully run, so such an approach was abandoned.

Since the model only allows the polymer-penetrant partition function to vary between reactant and transition state, the ratio of partition functions would depend on the shape of the potential function for the penetrant in reactant and transition state, which means the identities of the neck and reactant cavity polymer atoms are needed as well as how close these atoms are to the penetrant. It needs to be pointed out that constructing such a model requires much detailed information from the simulations, making *a priori* predictions of *D*'s at this stage impossible.

6.3 Evaluating a Macroscopic *D* from a Distribution of Jumps

Once a model is provided to predict the parameters l, E_0 and Q^+/Q for a given jump, apart from doing a stochastic simulation, the distribution and connectivity of these jumps is required to get a macroscopic D. The simplest approach is to assume that jumps are uncorrelated. After a penetrant executes a jump, it can then execute any other jump in the simulated microstructure. A macroscopic D is then given by

$$D = \lim_{N\to\infty} \frac{1}{N} \sum_{i=1}^{N} P_i \frac{1}{n_i} \left[\sum_{j=1}^{n_i} \frac{k_{ij} l_{ij}^2}{6} \right] \tag{6.4}$$

where N is the number of cavities considered, n_i is the number of jumps from a particular cavity i, P_i is the probability of a penetrant occupying that cavity, and k_{ij} and l_{ij} are rate coefficients and jump lengths respectively. P_i would depend on how the selection of cavities is chosen, a selection intended to reflect reality. The uncorrelated approach does not allow for reverse jumps to occur.

One would expect successive jumps to be strongly correlated, and so knowing their connectivity is important. After a jump is executed by a penetrant, only a limited number of jumps are then available for the next jump, one of these being the reverse of the original jump. Even though a certain type of jump might be found in many places in a polymer, this does not mean that penetrants will execute it proportionally as many times. For example, there could be a lot of slow jumps, but all it takes is a few quick jumps to bypass the slow ones, and on the other hand, a rare but slow jump could act as a bottleneck. And of course, faster jumps will be executed more often than slower ones, even if they are in equal numbers. The type of jumps that lead to a particular reactant cavity of a jump should strongly determine the likelihood of that jump itself occurring. An analysis obtaining this information, while laborious, is possible in principle and it may be possible to extract some simple empirical rules. However, a formula for D by this approach currently is unknown. It is likely to be highly recursive in nature. Nevertheless, a macroscopic D should still be possible to obtain from a stochastic simulation (e.g. June *et al.*, 1991) on a large enough box.

6.4 Evaluating the Ratio of Partition Functions

An attempt was made to evaluate the ratio of the transition state partition function to the reactant one. It can be seen from Figure 6.1 that the frequency number distribution of the normal modes for reactant, transition state and product obtained from Greenfield and Theodorou's simulations are extremely similar.

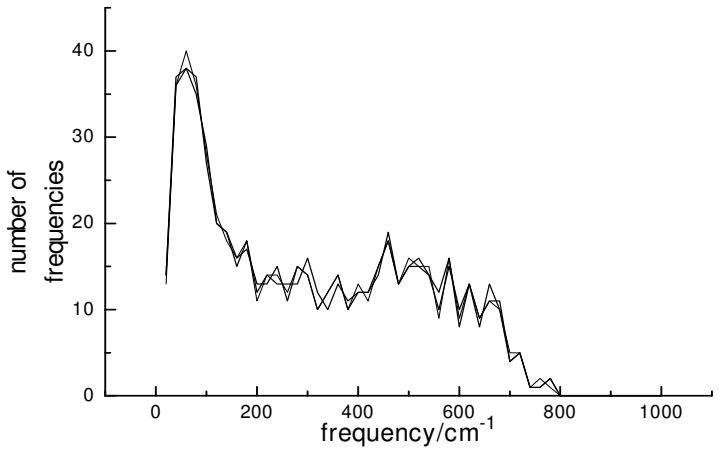

Figure 6.1: Graph of the number distribution of frequencies from normal mode analysis versus frequencies for reactant, transition state and product systems. What is striking is not so much which one is which, but the similarity between them.

It is the differences in these plots that determine what the partition function ratio will be. It was theorised that these differences would show up in the respective normal modes. Some relationship might then be found to explain why their frequencies are different. Appendix D addresses in brief attempts to do this. However, as might be expected for normal modes in such a highly coupled and high-dimensional system, there were many differences, none of which could be specifically characterised. Thus the approach described in Chapter 5.4 was the best that could be done.

Chapter 7

Conclusion

A model to describe the diffusion mechanism of small molecules in amorphous glassy polymers has been put forward. The model has no adjustable parameters, and only requires one parameter to be provided for it from simulations, which is r_0, the radius of the largest percolating penetrant. Knowledge of this parameter only requires a geometric analysis of unoccupied volume, not a full TST calculation. Even if r_0 is not known for a particular system, the model can still be used to fit experimental data and predict trends with penetrant size (for example, scaling D of penetrant with tracer dyes (Tonge, in progress) used in FRS experiments (Section 3.2)) and temperature. While the D predicted by the model for methane in polypropylene at 233 K could not be compared with an experimental measurement, the order of magnitude agreement with methane in poly(vinyl chloride) at 298K is encouraging. The model's prediction of the Arrhenius dependence of D on temperature compares well with experiment. A comparison of its prediction of the dependence of D on penetrant size with experiment is reasonable for small penetrants ($\sigma < 4.5$ Å), but drops away by orders of magnitude for larger penetrants.

Attempts were made to incorporate more of the variation and realism shown in the simulations. However, no complete models could be formed either to quantify the required parameters for each type of jump or to put those jumps together to obtain a macroscopic D. Future work should first of all involve calculating more accurately the parameters for the average jump. These include a more accurate form of $V_{popo}(r)$ for the average jump using the theory of elastic solids (Section 6.1) and a procedure to understand and ideally quantify the ratio of partition functions of the whole system (Section 6.4). Secondly, the validity of the approximation of the average jump (Section 5.1) should be more thoroughly investigated and whether the features chosen for this jump by the model match it. Thirdly, the model should be expanded to calculate parameters for different jumps (Section 6.2). And finally, the distribution and connectivity of jumps themselves would have to be examined in order to calculate a macroscopic D (Section 6.3). Advancement of such an approach would require a much more extensive analysis of computer simulations.

Nevertheless, with verification from the computer simulations of Greenfield and Theodorou, the proposed model captures the basic and most important elements of the diffusion mechanism.

Appendix A: Generation of Polymer Structures

There are three main techniques to generate initial polymer microstructures. These are:

1. a modified version of Flory's rotational isomeric state model (Flory, 1969) that takes into account non-bonded interaction (Theodorou and Suter, 1985).
2. gradually "turning on" bonds between a liquid of united atoms (Rigby and Roe, 1987).
3. using a regular crystalline lattice (Pant and Boyd, 1991).

Methods used to equilibrate the generated structures are:

1. Energy minimisation (Theodorou and Suter, 1985).
2. Monte-Carlo simulations using a random series of moves, either reptations (Pant and Boyd, 1991) or concerted rotations (Dodd *et al.*, 1995).
3. Molecular dynamics simulations, involving alternately cooling and re-equilibrating the structure (Rigby and Roe, 1987).

Appendix B: Stochastic Simulations

A certain number of non-interacting penetrants are put in the polymer. Each jump from cavity *A* to cavity *B* is assumed to be a first-order process, with rate coefficient k_{AB}. If there are N possible moves for all of particles put together, the overall rate coefficient of the system is given by

$$\rho = \sum_{i=1}^{N} (k_{AB})_i \tag{B.1}$$

The probability that a particular *i*th event will next occur is equal to $(k_{AB})_i/\rho$. Assuming that the times between jumps obey Poisson statistics, the time for this next randomly chosen event to occur is given by

$$\tau = \frac{\ln(1-\xi)}{-\rho} \tag{B.2}$$

where ξ is random number between 0 and 1. After many such steps, a diffusion coefficient is then obtained by using Eq. 4.10.

Appendix C: Calculating *k* using TST

This summarises the method of Greenfield and Theodorou. Initial cartesian coordinates, **x**, for polymer atoms are mass-weighted ($\mathbf{x}_m = m^{1/2}\mathbf{x}$, where m is the mass of the atom whose coordinate it is). Coordinates are then transformed to bond vectors, **y**, which are then transformed to generalised coordinates, **q**. These comprise the x, y and z of the penetrant (when introduced into the polymer), x, y and z of all three chain starts, the Euler angles of the first bond of each chain (with respect to the simulation box), and bond and torsional angles. Such a transformation is necessary, since the potential is defined in terms of these coordinates.

An initial guess for the transition state is the two-dimensional surface at the narrowest part in a neck connecting two cavities. The penetrant is then placed at this surface, and the transition state with respect to the three penetrant degrees of freedom is found using Baker's algorithm (Baker, 1986). Then, the more accurate transition state much lower in energy is found by also incorporating flexible polymer degrees of freedom, again using Baker's algorithm. The transition state is the point at which the gradient of the potential is zero, and one of the eigenvalues of the Hessian matrix, H_{qq}, the matrix of second derivatives of potential with respect to coordinates, is negative.

The next step involves finding the intrinsic reaction coordinate (IRC) (Fukui, 1987) , or the minimum energy path, which leads from the transition state on either side to reactant and product minima. The first step, $d\mathbf{q}$, from the transition state is found by taking a step in the direction of the negative eigenvalue, λ, which is found by solving the generalised eigenvalue equation

$$\mathbf{H}_{qq} d\mathbf{q} = \lambda \mathbf{a} d\mathbf{q}, \tag{C.1}$$

where a is the metric tensor, defined as

$$a_{ij} = \sum_k \frac{\partial x^k}{\partial q^i} \frac{\partial x^k}{\partial q^j}. \tag{C.2}$$

Subsequent steps are then taken down the steepest descent path, found by solving

$$\mathbf{a} d\mathbf{q} = \nabla_q V d\tau, \tag{C.3}$$

where $\nabla_q V$ is the gradient of the potential and $d\tau$ is a scaling constant. The first minima found on either side are taken as reactant and product minima. Both minima are useful, since a forward jump is equally as valid as a backward jump.

Having found reactants and transition states, E_0 is just the difference in energy between their minima on the potential energy surface. To find the partition functions at each place, the harmonic approximation for the potential is used. This enables the polymer's motion to be described as vibrations of normal modes, the partition functions of which can be calculated. Note that the dimensionality of the minimum of the transiton state is f-1, one less than that for the reactant minimum, as the remaining coordinate is the reaction coordinate. The harmonic approximation is a second order truncation of a Taylor expansion of the potential about the minimum, $\mathbf{q} = \mathbf{q}_0$, namely

$$V(\mathbf{q}) \approx V(\mathbf{q}_0) + \tfrac{1}{2}(\mathbf{q}-\mathbf{q}_0)^T \mathbf{H}_{qq}(\mathbf{q}-\mathbf{q}_0), \qquad \text{(C.4)}$$

where the first order term is zero, since the gradient of the potential at a minimum is zero, and T indicates the *transpose*. Eigenvectors (normal modes) and their eigenvalues, λ_i, (force constants of normal modes), are found by solving the generalised eigenvalue equation (Eq. C.1). After transforming generalised coordinates to normal coordinates, and obtaining the frequencies of the normal modes using the equation

$$\nu_i = \sqrt{\lambda_i} \,/\, 2\pi, \qquad \text{(C.5)}$$

the reactant partition function is given by a product of vibrational partition functions

$$Q = \prod_{i=1}^{f} \left(1 - \exp\left(\frac{-h\upsilon_i}{k_B T} \right) \right)^{-1}. \qquad \text{(C.6)}$$

The formulae for the transition state partition function is the same, except that there are f-1 degrees of freedom.

Appendix D: Mechanical Engineering Approach to Calculating $V_{\mathbf{popo}}(r)$

This specifies a method to be used for a more advanced treatment of $V_{popo}(r)$ to replace the one developed in Section 5.3. Because of time constraints, the required development is yet to be carried out. The problem of calculating the energy to expand a

cylinder is referred to by engineers as the "thick walled cylindrical pressure vessel" problem, or the Lamé problem (Tanner *et al.*; 1990, Zhang, 1994; Popov, 1990).

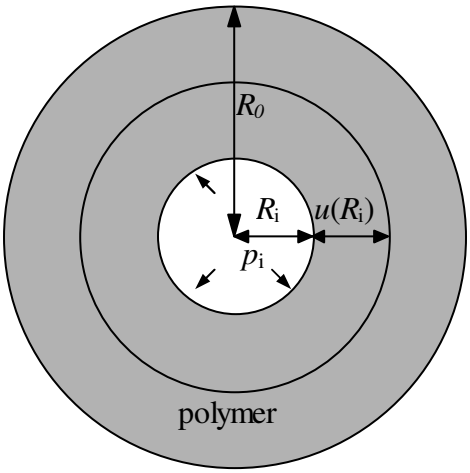

Figure D.1: Cross-section of the hollow cylindrical polymer pipe. R_0 and R_i are outer and inner radii. p_i is the pressure applied to the inner surface.

The polymer is treated as a hollow pipe (Figure D.1). R_0 and R_i are outer and inner radii of the polymer pipe respectively. When a pressure, p_i, is applied to the polymer from the inside, the inner radius expands. The change in radial displacement, $u(r)$, for a point at radius r is given by

$$u = A_1 r + A_2 / r \tag{D.1}$$

where

$$A_1 = \frac{(1+\nu)(1-2\nu)}{E} \frac{p_i^2 r_i^2}{r_0^2 - r_i^2} \tag{D.2}$$

and

$$B = \frac{(1+\nu)}{E} \frac{p_i r_i^2 r_0^2}{r_i^2 - r_0^2} \tag{D.3}$$

where ν is Poisson's ratio and E is Young's modulus. The expansion of the inner radius is equal to $u(R_i)$. Hence, if the neck is to be expanded by $u(R_i)$, then Eq. D.1 can be used to calculate p_i, the pressure required to do this.

Using cylindrical coordinates, the stresses, σ, and strains, ε, are given by

$$\sigma_r = \frac{p_i r_i^2}{r_0^2 - r_i^2} \left(1 - \frac{r_0^2}{r^2}\right) \tag{D.4}$$

$$\sigma_\theta = \frac{p_i r_i^2}{r_0^2 - r_i^2}\left(1 + \frac{r_0^2}{r^2}\right) \tag{D.5}$$

$$\varepsilon = \frac{\partial u}{\partial r} \tag{D.6}$$

$$\varepsilon = \frac{u}{r} \tag{D.7}$$

(all other stresses and strains are zero by symmetry). In a linear elastic solid, the strain energy per unit volume in cartesial coordinates is given by

$$W = \tfrac{1}{2}\left(\sigma_{xx}\varepsilon_{xx} + \sigma_{yy}\varepsilon_{yy} + 2\sigma_{xy}\varepsilon_{xy}\right). \tag{D.8}$$

Stresses can be converted from cylindrical coordinates using the transformations

$$\sigma_{xx} = \tfrac{1}{2}\left(\sigma_r + \sigma_\theta\right) + \tfrac{1}{2}\left(\sigma_r - \sigma_\theta\right)\cos 2\theta \tag{D.9}$$

$$\sigma_{yy} = \tfrac{1}{2}\left(\sigma_r + \sigma_\theta\right) - \tfrac{1}{2}\left(\sigma_r - \sigma_\theta\right)\cos 2\theta \tag{D.10}$$

$$\sigma_{xy} = \tfrac{1}{2}\left(\sigma_r - \sigma_\theta\right)\sin 2\theta. \tag{D.11}$$

The total strain energy in the polymer is then given by

$$U = \int_0^L \int_{-\infty}^{\infty} \int_{-\infty}^{\infty} W dx dy dz \tag{D.12}$$

where L is taken as the length of the cylinder as in Chapter 5. R_0 is chosen to be extremely large (effectively at infinity), and R_i is taken as the pre-existing neck radius.

Appendix E: Analysis of System Partition Function

By examining the normal modes from the simulations (Greenfield and Theodorou, 1995b), it was hoped that differences in the characteristic motions of the polymer might be found between reactant and transition state, as is commonly done for unimolecular reactions (Gilbert and Smith, 1990). Such a difference might include the penetrant and the surrounding atoms being unable to move very much in the transition state, or at least, they would move more in unison. This would be expected to show up as differences in displacements in the normal modes.

In order to see differences in normal modes, it is helpful to find the normal modes that do not change. In collaboration with Greenfield and Theodorou, the dot

product was taken between all possible pairs of normal modes for reactant and transition state. The closer the dot product of a pair of normal modes is to one, the more identical they are. It was found that the pairs with the largest dot products were always of normal modes with similar frequency. Many of the reactant normal modes were very similar in character to one of the transition state normal modes (dot product between 0.5 and 1). However, some normal modes dotted significantly with more than one transition state mode, suggesting extensive coupling. It was also found that the transition state normal mode with the negative eigenvalue (imaginary mode), corresponding to the penetrant jumping over the barrier, dotted with many reactant modes, but only those of low frequency (<100 cm^{-1}).

Participation ratios were also looked at (Bell *et al.*, 1970). A participation ratio is the fraction of total atoms in the system effectively taking part in the normal mode. They give an idea of the localisation of the mode. It was found that most normal modes had participation ratios between 0.08 and 0.3. The only interesting feature that could be picked out from this approach was that the imaginary mode had a participation ratio of 0.0016. Given that there are about 900 atoms in the system, this implies that 1.4 atoms effectively take part in the imaginary mode. This one atom is probably the penetrant.

Another method was to examine the frequency number distribution (Figure 6.1) for differences in the frequencies between reactant and transition state and consider the normal modes of these particular frequencies. The different motions of these normal modes were expected to characterise the differences between reactant and transition state.

Overall, the analysis provided some insight into the partition functions of reactant and transition state. However, a complete procedure to understand and quantify the ratio of partition functions was not achieved.

References

Baker, J. *J. Comput. Chem.* **1986**, *7*, 385.

Barrer, R. M. *Trans Faraday Soc.* **1943**, *39*, 48.

Barrer, R. M. *Nature* **1937**, *140*, 106.

Barrer, R. M. *Trans Faraday Soc.* **1939a**, *35*, 629.

Barrer, R. M. *Trans Faraday Soc.* **1939b**, *35*, 644.

Barrer, R. M. *J. Phys. Chem.* **1957**, *61*, 178.

Bell, R. J., Dean, P., Hibbins-Buttler, D. C. *J. Phys. C: Solid St. Phys.* **1970**, *3*, 2111.

Boone, T., D. Ph.D. Thesis., Uni. of California (Berkeley), **1995.**

Brandt, W. W. *J. Phys. Chem.* **1959**, *63*, 1080.

Chandresekhar, S. *Rev. Mod. Phys.* **1943**, *15*, 1.

Cohen, M. H., Turnbull, D. *J. Chem. Phys.* **1959**, *31*, 1164.

DiBenedetto, A. T. *J. Polym. Sci.* **1963**, *A1*, 3477.

Dodd, L. R., Boone, T. D., Theodorou, D. N. *Mol. Phys.* **1993**, *78*, 961.

Doolittle, A. K., *J. Appl. Phys.* **1951**, *22*, 1471.

Ehlich, D., Sillescu, H. *Macromolecules* **1990**, *23*, 1600.

Flory, P. J. *Statistical Mechanics of Chain Molecules* **1969**, Wiley-Interscience, New York; Chapters 1,3.

Frick, T. S., Huang, W. J., Tirrell, M., Lodge, T. P. *J. Polym. Sci., Polym. Phys. Ed.* **1990**, *28*, 2629.

Fukui, K. *Acc. Chem. Res.* **1981**, *14*, 364.

Fujita, H. *Fortschr. Hochpolym.-Forsch.* **1961**, *3*, 1.

Furuya, H., Mondello, M., Yang, H.-J., Roe, R.-J., Erwin, R. W., Han., C. C., Smith, S. D. *Macromolecules* **1994**, *27*, 5674.

Gilbert R. G., Smith S. C. *Theory of Unimolecular and Recombination Reactions* **1990**, Blackwell, Oxford.

Gilbert, R. G., *Emulsion Polymerization* **1995**, Academic Press, Oxford.

Go, N., Scheraga, H. A. **1976**, *9*, 535.

Greenfield, M. L.; Theodorou, D. N. *Macromolecules* **1993**, *26*, 5461.

Greenfield, M. L.; Theodorou, D. N. *Polym. Mat. Sci. and Eng. (Am. Chem. Soc.)* **1994**, *71*, 407.

Greenfield, M. L.; Theodorou, D. N. *Polym. Prepr., Am. Chem. Soc., Div. Polym. Chem.* **1995a**, *36*, 687.

Greenfield, M. L.; Theodorou, D. N. private communication **1995b**.

Gusev, A. A., Arizzi, S., Suter, U. W. *J. Chem. Phys.* **1993**, *99*, 2221.

Gusev, A. A., Suter, U. W. *J. Chem. Phys.* **1993**, *99*, 2228.

Gusev, A. A., Müller-Plathe, F., van Gunsteren, W. F., Suter, U. W. *Adv Polym. Sci.* **1994**, *116*, 207.

Huang, W. J., Frick, T. S., Landry, M. R., Lee, J. A., Lodge, T. P., Tirrell, M. *AIChE J.* **1987**, *33*, 573.

June, R. L., Bell, A. T., Theodorou, D. N. *J. Phys Chem.* **1991**, *95*, 8866.

Koros, W. J., Fleming, G. K., Jordan, S. M., Kim, T. H., Hoehn, H. H. *Prog. Polym. Sci.* **1988,** *13*, 339.

Kovacs *J. Polym. Sci.* **1958**, *30*, 131.

Kreituss, A., Frisch, H. I. *J. Polym. Sci., Polym. Phys. Ed.* **1981**, *19*, 889.

Lind, J. H., Jones, P. L., Pearsall, G. W. *J. Polym. Sci., Polym. Chem. Ed.* **1986**, *24*, 3033.

Meares, P. *J. Am. Chem. Soc.* **1954**, *76*, 3415.

Meares, P. Trans. *Faraday Soc.* **1957**, *53*, 101.

Miller, W. H. *J. Chem. Phys.* **1982**, *76*, 4904.

Müller-Plathe, F. *J. Chem. Phys.* **1991**, *94*, 3192.

Müller-Plathe, F. *J. Chem. Phys.* **1992,** *96*, 3200.

Müller-Plathe, F., Rogers, S. C., van Gunsteren, W. F. *Macromolecules* **1992**, *25*, 6722.

Müller-Plathe, F., Rogers, S. C., van Gunsteren, W. F. *J. Chem. Phys.* **1993a**, *98*, 9895.

Müller-Plathe, F., Laaksonen, L, van Gunsteren, W. F. *J. Mol. Graph.* **1993b**, *11*, 118.

Pace, R., Datyner, A. *J. Polym. Sci., Polym. Phys. Ed.* **1979a**, *17*, 437.

Pace, R., Datyner, A. *J. Polym. Sci., Polym. Phys. Ed.* **1979b**, *17*, 453.

Pace, R., Datyner, A. *J. Polym. Sci., Polym. Phys. Ed.* **1979c**, *17*, 465.

Pant, P. V. K., Boyd, R. H. *Macromolecules* **1991**, *24*, 6325.

Pant, P. V. K., Boyd, R. H. *Macromolecules* **1992**, *25*, 494.

Pant, P. V. K., Boyd, R. H. *Macromolecules* **1993**, *26*, 679.

Paul, D. R., Koros, W. J. *J. Polym. Sci., Polym. Phys. Ed.* **1976**, *14*, 675.

Pickup, S., Blum, F. D. *Macromolecules*, **1989**, *22*, 3961.

Piton, M. C., Gilbert, R. G., Chapman, B. E., Kuchel, P. W. *Macromolecules*, **1993**, *26*, 4472.

Popov, E. P. *Engineering Mechanics of Solids* **1990**, Prentice-Hall, New Jersey; p 159.

Rice, S. A., *Quantum Dynamics of Molecules* **1980**, ed. R.G. Woolley; Plenum: New York; p 257.

Rigby, D., Roe, R-J. *J. Chem. Phys.* **1987**, *87*, 7285.

Rigby, D., Roe, R. J. *Macromolecules* **1990**, *23*, 5312.

Roe, R. J. *Adv. Polym. Sci.* **1994**, *116*, 111.

Ryckaert, J-P., Ciccotti, G., Berendsen, H. J. C. *J. Comp. Phys.* **1977**, *23*, 327.

Schaefer, D., Spiess, H. W., Suter, U. W., Fleming, W. W. *Macromolecules* **1990**, *23*, 3431.

Sok, R. M., Berendsen, H. J. C., van Gunsteren, W. F. *J. Chem. Phys.* **1992**, 96, 4699.

Sonnenburg, J., Gao, J., Weiner, J. H. *Macromolecules* **1990**, *23*, 4653.

Stannet, V., Crank, J., Park, G. S. *Diffusion in polymers*, Academic press: New York, **1968**, Chapter 3.

Stern, S. A., Frisch, H. L. *Ann. Rev. Mater. Sci.* **1981**, *11*, 523.

Takeuchi, H., Okazaki, K. *J. Chem. Phys.* **1990**, *92*, 5643.

Takeuchi, H. *J. Chem. Phys.* **1990a**, *93*, 2062.

Takeuchi, H. *J. Chem. Phys.* **1990b**, *93*, 4490.

Takeuchi, H., Roe, R., Mark, J. E. *J. Chem. Phys.* **1990**, *93*, 9042.

Takeuchi, H., Roe, R. *J. Chem. Phys.* **1991**, *94*, 7458.

Takeuchi, H., Okazaki, K. *Makromol. Chem., Macromol. Symp.* **1993**, *65*, 81.

Tamai, Y., Tanaka, H., Nakanishi, K. **1994**, *27*, 4498.

Tanemura, M., Ogawa, T., Ogita, N. *J. Comput. Phys.* **1983**, *51*, 191.

Tanner, R. I. *et al*. *Notes on Mechanics of Solids* **1990**, Sydney University Printing Service; p 112.

Theodorou, D. N., Suter, U. W. *Macromolecules* **1985** ,*18*, 1467.

Tonge, M. P. in progress.

Trohalaki, S., Rigby, D., Kloczkowski, A., Mark, J. E., Roe, R. J. *Polym. Prepr. (Am. Chem. Soc., Div. Polym. Chem.)* **1989**, *30*, 23.

Verlet, L. *Phys. Rev.* **1967**, *159*, 98.

Vineyard, G. *J. Phys.Chem. Solids* **1957**, *3,* 121.

Vrentas, J. S., Duda, J. L. *J. Polym. Sci., Polym. Phys. Ed.* **1977a**, *15*, 403.

Vrentas, J. S., Duda, J. L. *J. Polym. Sci., Polym. Phys. Ed.* **1977b**, *15*, 417.

Vrentas, J. S., Duda, J. L. *J. Polym. Sci., Polym. Phys. Ed.* **1977c**, *15*, 441.

Vrentas, J. S., Duda, J. L., Ling, H.-C. *J. Polym. Sci., Polym. Phys. Ed.* **1988**, *26*, 1059.

Vrentas, J. S., Chu, C.-H., Drake, M. C.,v. Meerwall, E. *J. Polym. Sci., Polym. Phys. Ed.* **1989**, 27, 1179.

Vrentas, J. S., Vrentas, C. M. *J. Polym. Sci, Polym. Phys. Ed.* **1993**, *31*, 69.

Williams, M. L., Landel, R. F., Ferry, J. D. *J. Am. Chem. Soc.* **1955**, *77*, 3701.

Zhang, J., Wang, C. H., Ehlich, D. *Macromolecules* **1986**, *19*, 1390.

Zhang, L. *Mechanics and Properties of Solids 2, Basic Equations, Formulae and Concepts*, **1994**.